Magnetic Energy Conversion Processes in the Sun & Planets

Planetary Magnetospheres

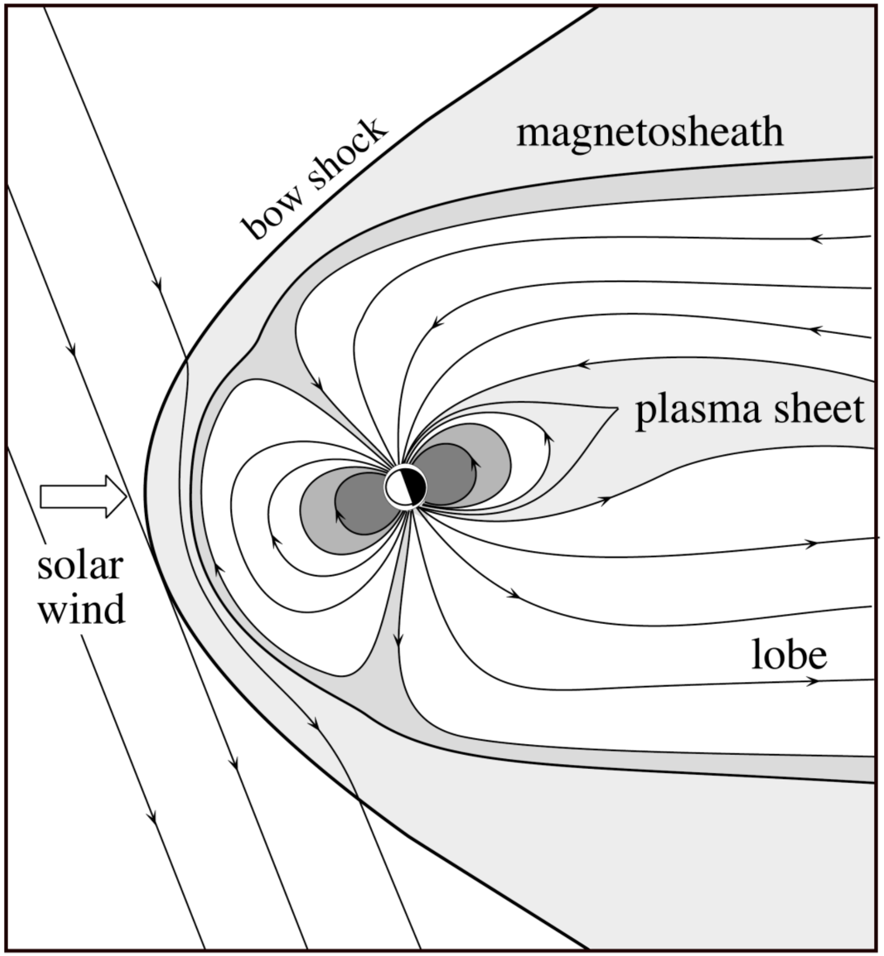

Solar Eruptions

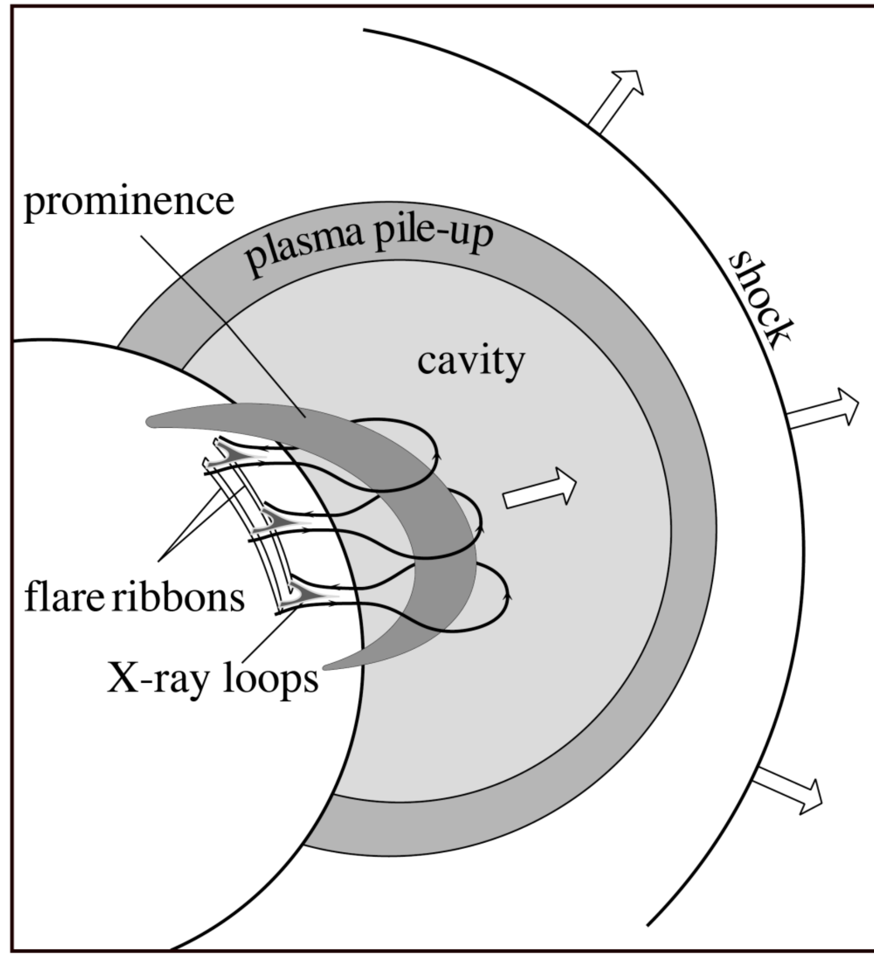

Comparison of Plasma Environments

Parameter	Terrestrial Plasma Sheet	Solar Active Region
L	10^{7} m	10^{8} m
n	10^{5} m^{-3}	10^{15} m^{-3}
B	10^{-8} Tesla	10^{-2} Tesla
ion-gyro radius / L	10^{-2}	10^{-9}
ion-inertial length /L	10^{-1}	10^{-7}
collisional mfp / L	10^{9}	10^{-4}
$V_A B / E_{\mathrm{Dreicer}}$	10^{11}	10^{7}

Evolutionary Phases for CMEs

1. Energy storage:

force-free fields:

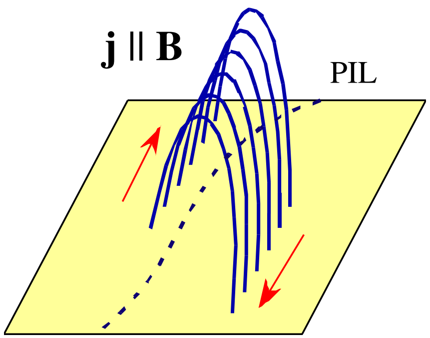

sheared arcade

current sheets:

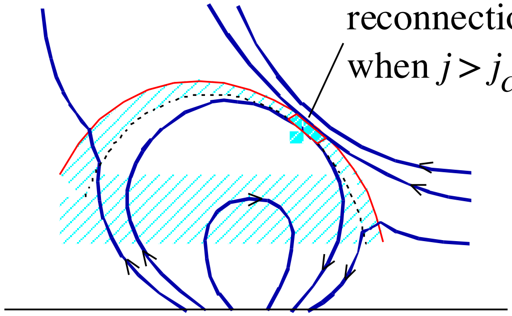

emerging flux model

2. Onset:

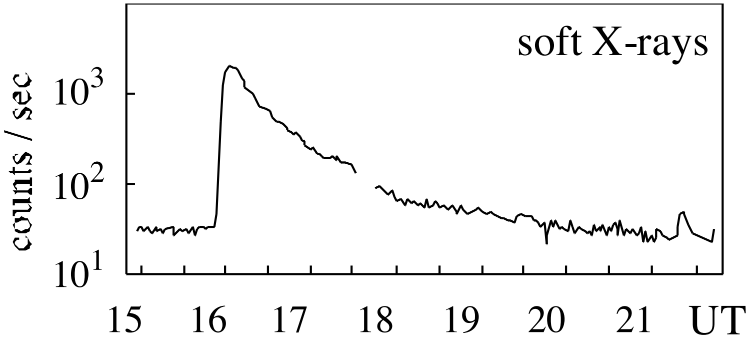

3. Recovery:

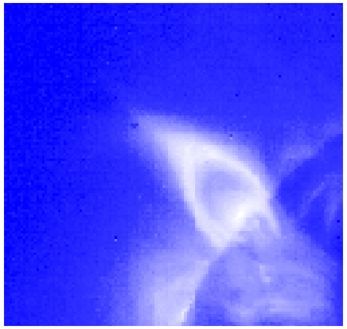

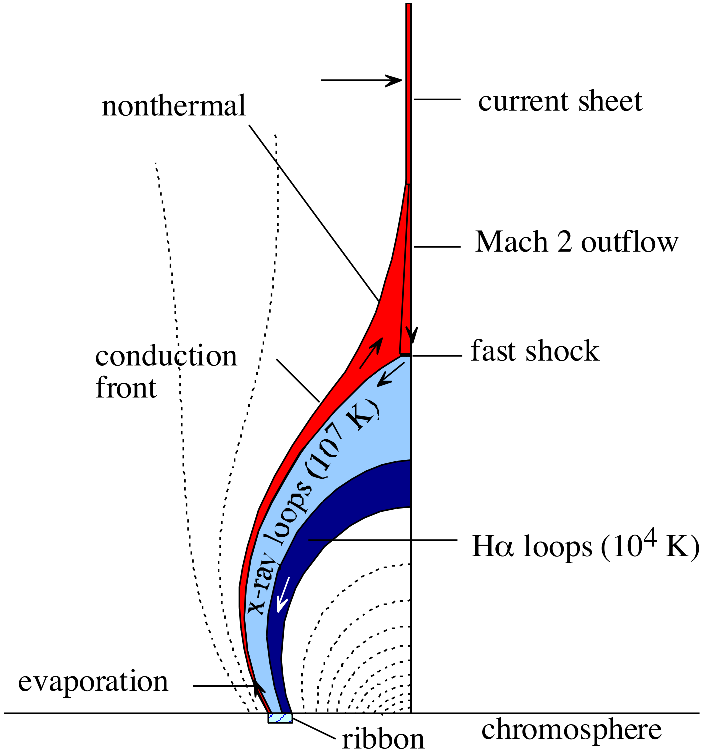

Energy Storage

CME/Flare Energetics

kinetic energy of mass motions: $\approx 10^{32}$ ergs

heating / radiation: $\approx 10^{32}$ ergs

work done against gravity $\approx 10^{31}$ ergs

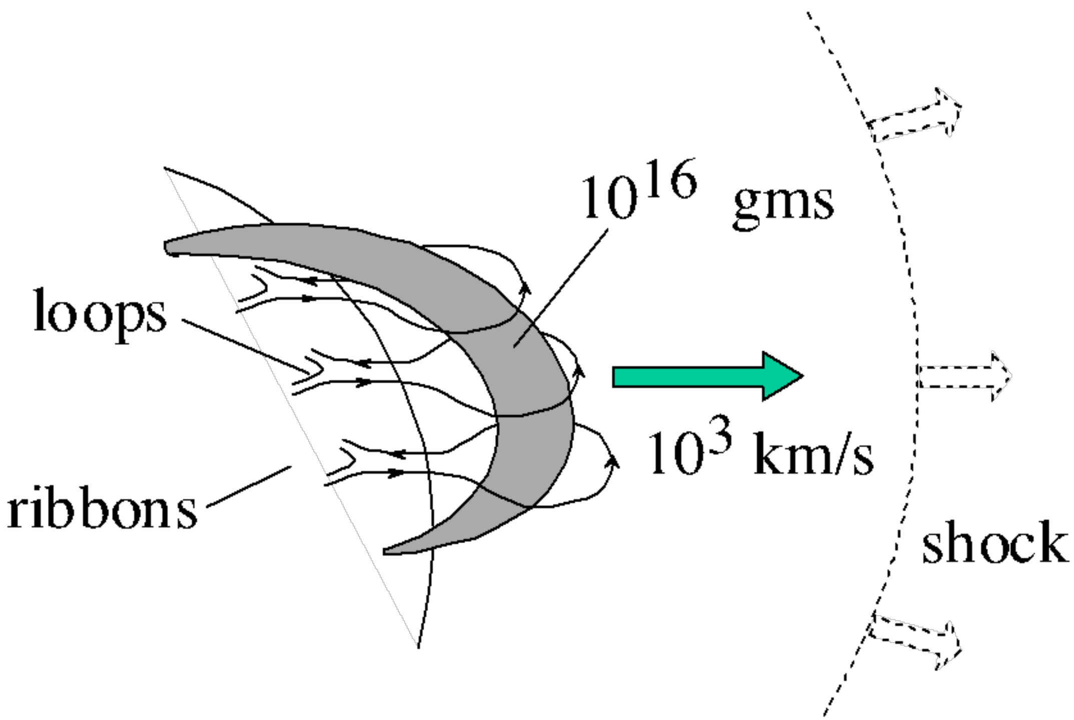

volume involved:
$\gtrsim (10^5\ \mathrm{km})^3$

energy density:
$\lesssim 100\ \mathrm{ergs/cm^3}$

Nature of Energy Source: Required: ≈ 100 ergs/cm^3

Type	Observed Values	Energy Density
kinetic $(m_p n V^2)/2$	$n = 10^9$ cm^{-3} $V = 1$ km/s	10^{-5} ergs/cm^3
thermal nkT	$T = 10^6$ K	0.1 ergs/cm^3
gravitational $m_p n g h$	$h = 10^5$ km	0.5 ergs/cm^3
magnetic $B^2/8\pi$	$B = 100$ G	400 ergs/cm^3

Apparent Motion of Loops & Ribbons

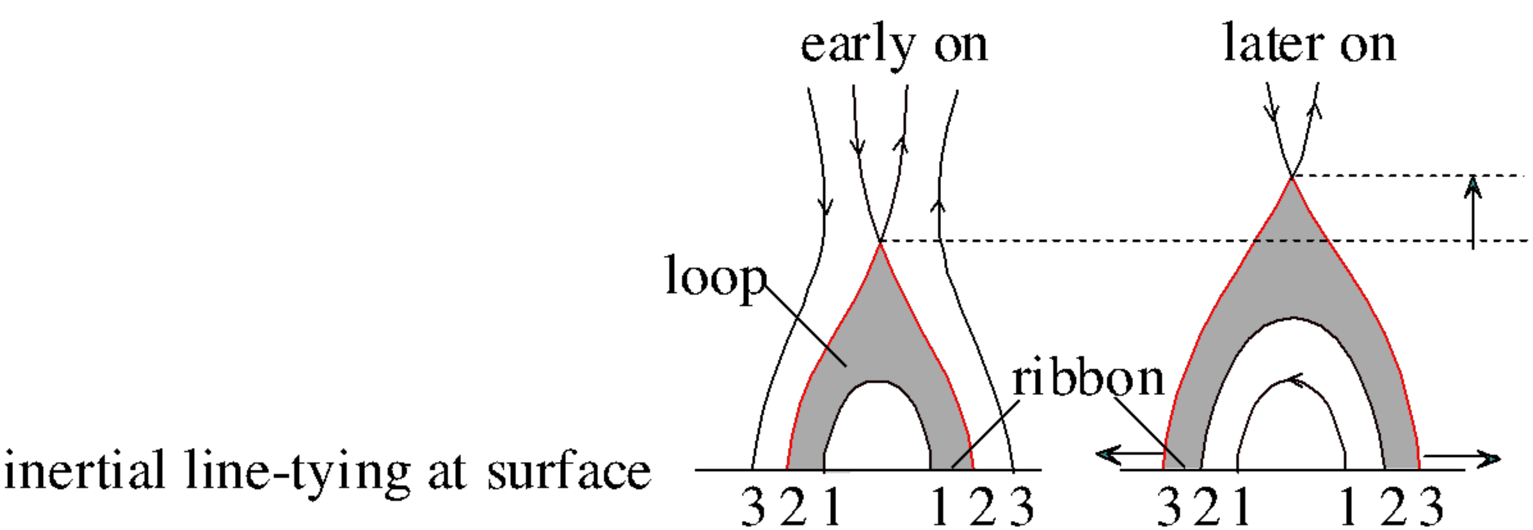

QuickTime™ and a
YUV420 codec decompressor
are needed to see this picture.

How Much Energy is Stored?

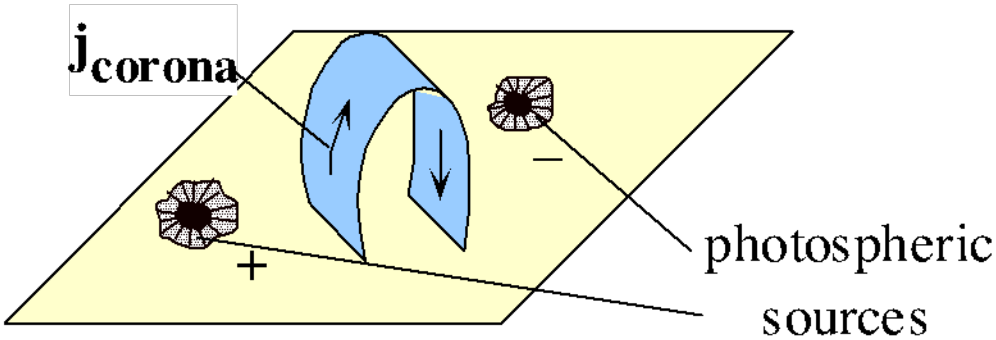

Hα image

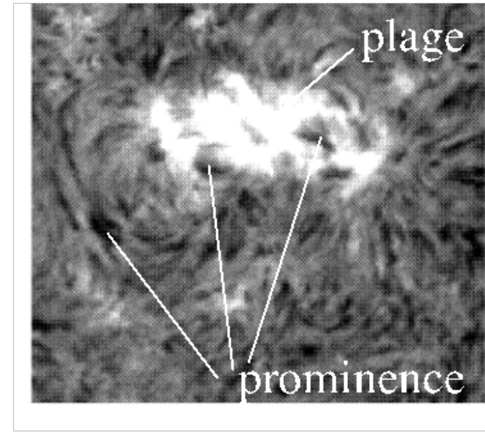

$$\mathbf{B} = \mathbf{B}_{\substack{\textbf{photospheric}\\\textbf{currents}}} + \mathbf{B}_{\substack{\textbf{coronal}\\\textbf{currents}}}$$

invariant during CME

source of CME energy

$$B_{\mathit{from\ corona}} \approx B_{\mathit{from\ photosphere}}$$

model with magnetogram

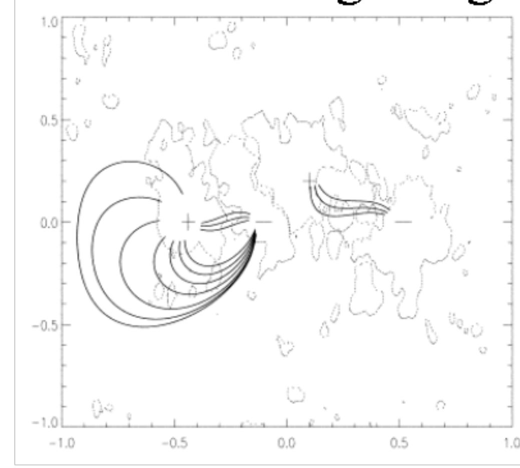

from Gaizauskas & Mackay (1997)

$\boxed{\text{free magnetic energy} \approx 50\% \text{ of total magnetic energy}}$

Aly - Sturrock Paradox

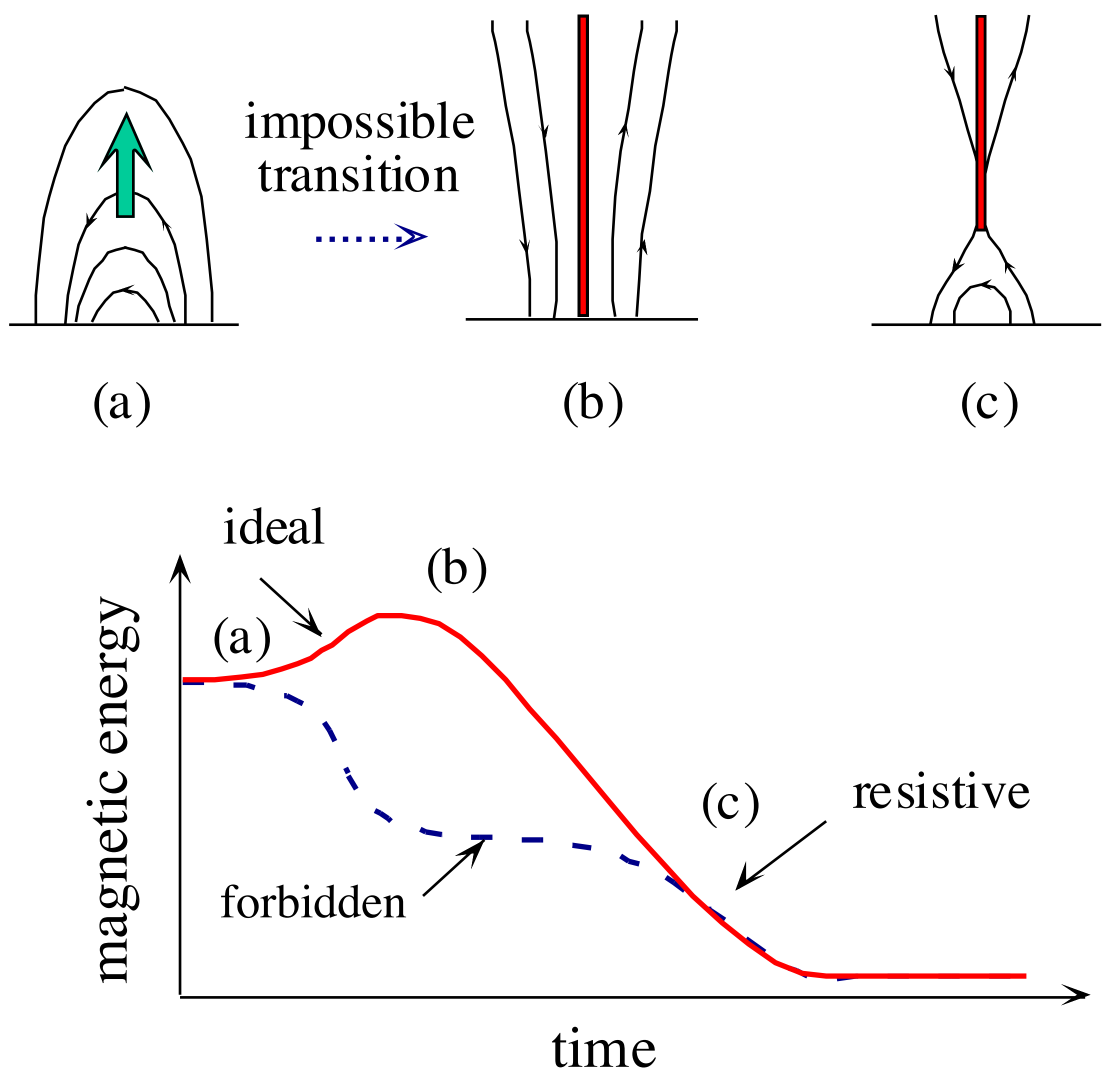

Flux Injection Models

(e.g. Chen 1989)

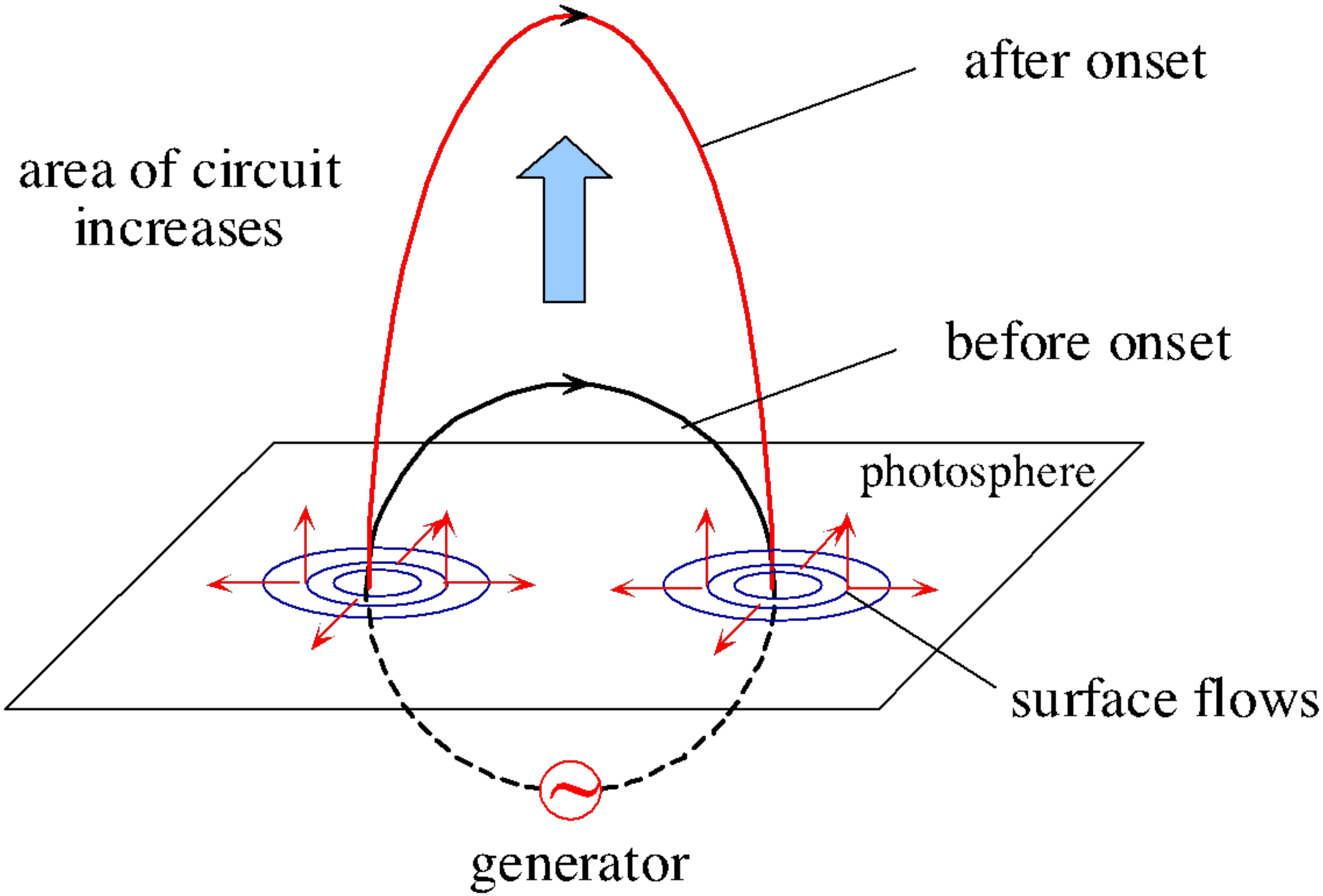

During injection energy flows through photosphere.

corona

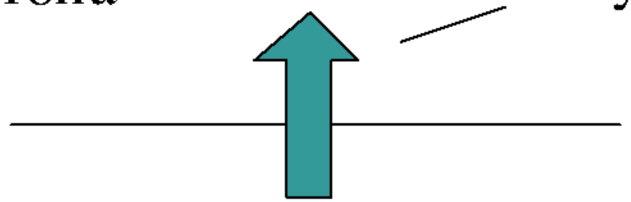

convection zone

Poynting flux:

$$\mathbf{S} = c\,\mathbf{E} \times \mathbf{B} \,/\, (4\pi)$$

(ergs/cm/sec)

$$\mathbf{E} = -(\mathbf{V} \times \mathbf{B}) \,/\, c$$

> 10 km/sec for > 10 minutes

Kosovichev et al. 1998

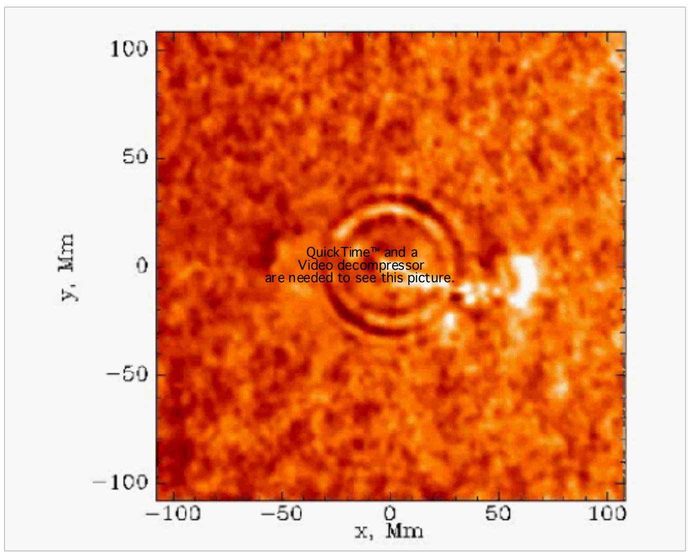

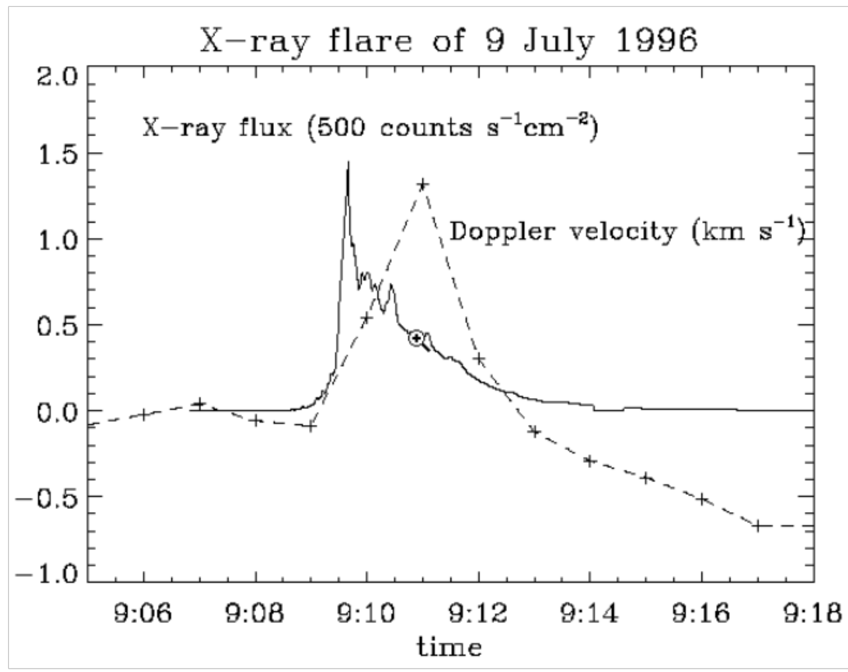

Injection models predict large surface flows which are never observed.

Substorm Energy Storage

solar wind kinetic energy converted to magnetic energy

SW kinetic energy

↓

magnetic energy

growth phase

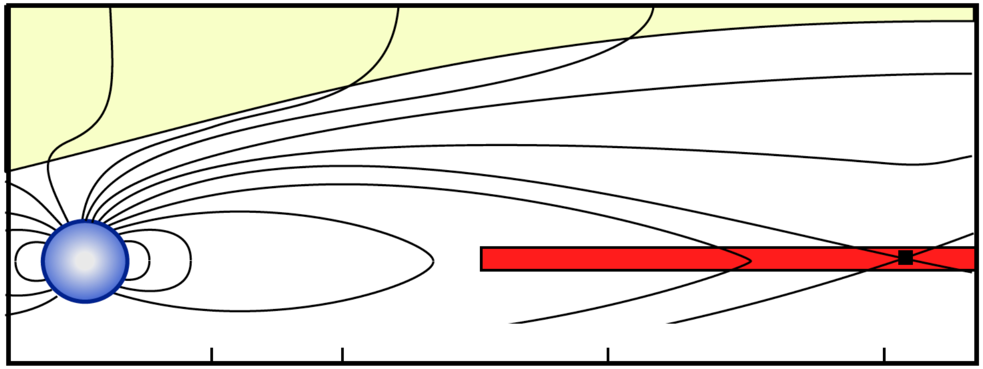

magnetic energy

↙ ↘

heat   kinetic

substorm onset

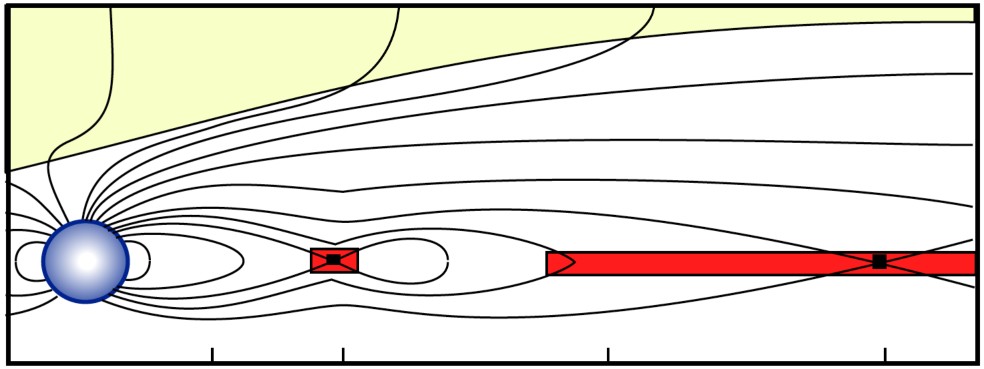

Evolutionary Phases for Substorm Plasmoid

1. Energy storage:
2. Onset:
3. Recovery:

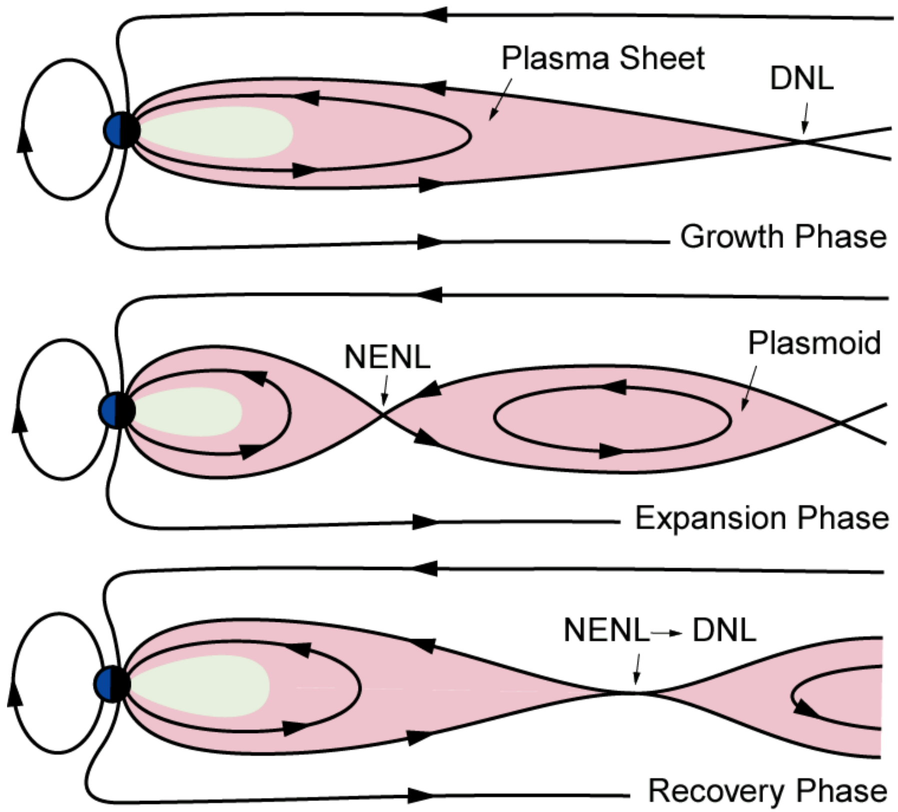

Commencement of Substorm Growth Phase

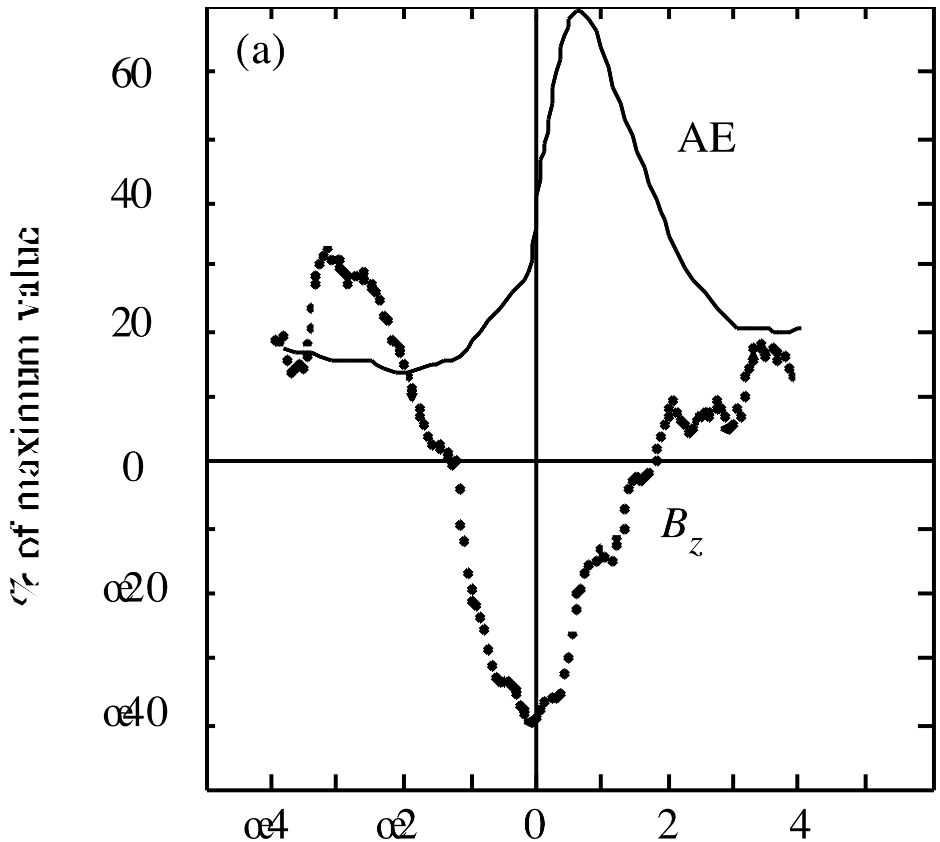

AE: Auroral Electroject Index

B_z: North-South Magnetic Field Component

Foster et al. 1971

2D Asymmetric Quadrupole Model

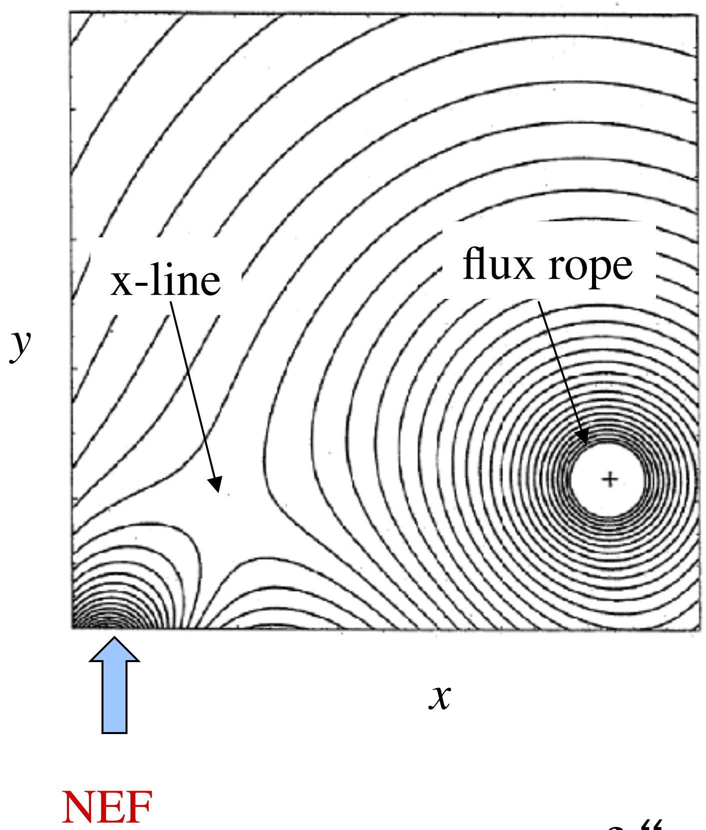

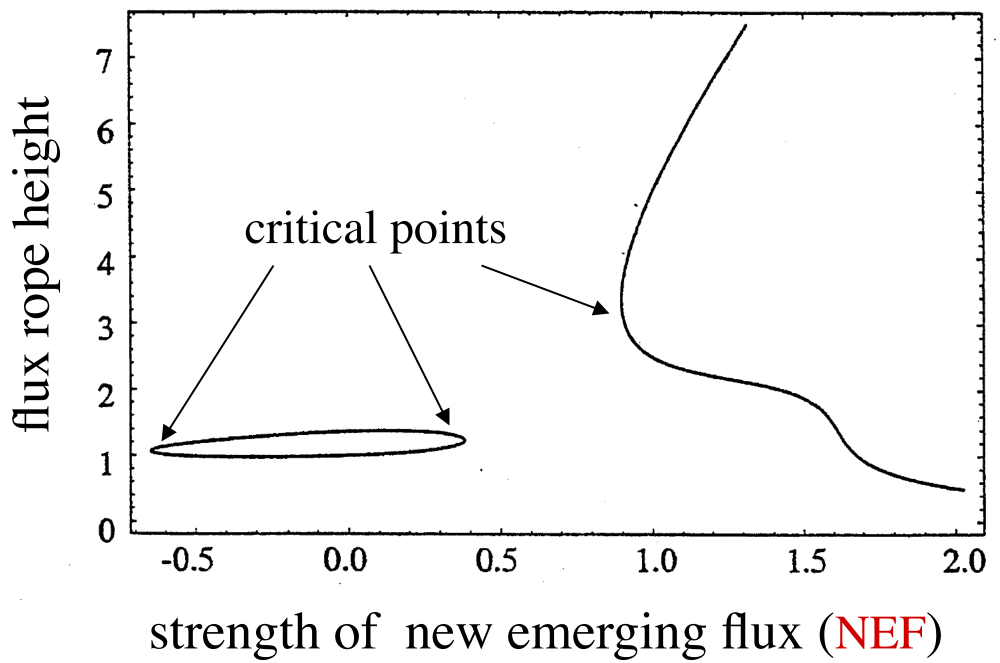

test of “tether-cutting” concept

Results From Feynman & Martin 1995

Table1.

Emerging Flux Near Filament?	Does the Filament Erupt Yes	No
Yes	17	5
No	5	26

Table2.

	Favorable for Reconnection	Unfavorable for Reconnection	Neither
Filament Erupted	17	2	2
Filament Did Not Erupt	0	3	3

Trigger Mechanism


Hα
Log (I / I_O)
0.5
original plage intensity

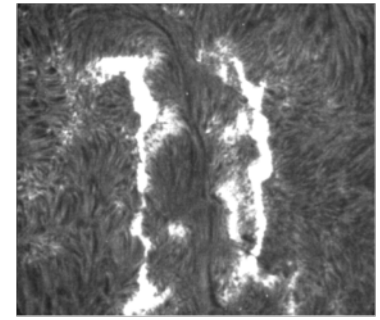

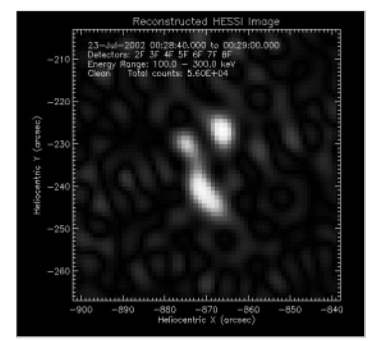
Reconstructed HESSI Image
23-Jul-2002 00:28:40.000 to 00:29:00.000
Detectors: 2F 3F 4F 5F 6F 7F 8F
Energy Range: 100.0 - 300.0 keV
Clean Total counts: 5.60E+04
Heliocentric Y (arcsec)
-210
-220
-230
-240
-250
-260
-900
-890
-880
-870
-860
-850
-840
Heliocentric X (arcsec)

Magnetic Energy Conversion:

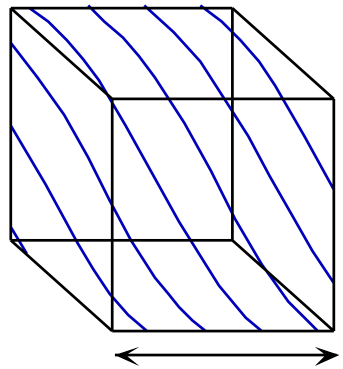

$L = 6 \times 10^4$ km

70 Gauss

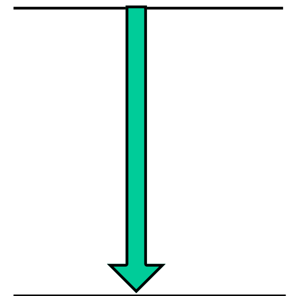

50 Gauss

$W_B = 10^{32}$ ergs

ideal MHD

reconnection

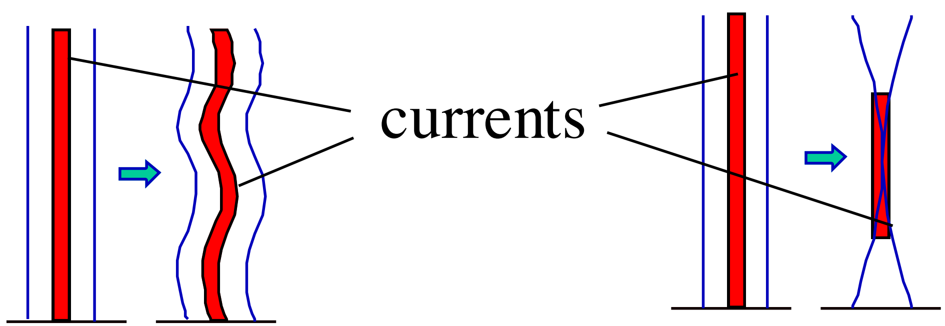

inefficient (< 10%)
fast

efficient (100%)
slow

Generalized Ohm's Law

$$\frac{4\pi}{\omega_{pe}^2}\frac{d\vec{J}}{dt} = \vec{E} + \frac{1}{c}\vec{v}_i \times \vec{B} - \frac{1}{nec}\vec{J} \times \vec{B} + \frac{1}{ne}\nabla \bullet \vec{\vec{p}}_e - \eta\vec{J}$$

electron inertia

advection Term

Hall term

electron stress

collisional resistivity

Origin of Non-Idealness

Comparison of non-ideal terms in Generalized Ohm's Law

Required Length to be Effective	Solar Corona		Terrestrial Magnetosphere	
inertia (λ_e)	10^{-1}	meters	10^{4}	meters
Hall (λ_i)	10^{1}		10^{6}	
e stress	10^{-3}		10^{5}	
collision	10^{-7}		10^{-7}	

Loss of Equilibrium Model

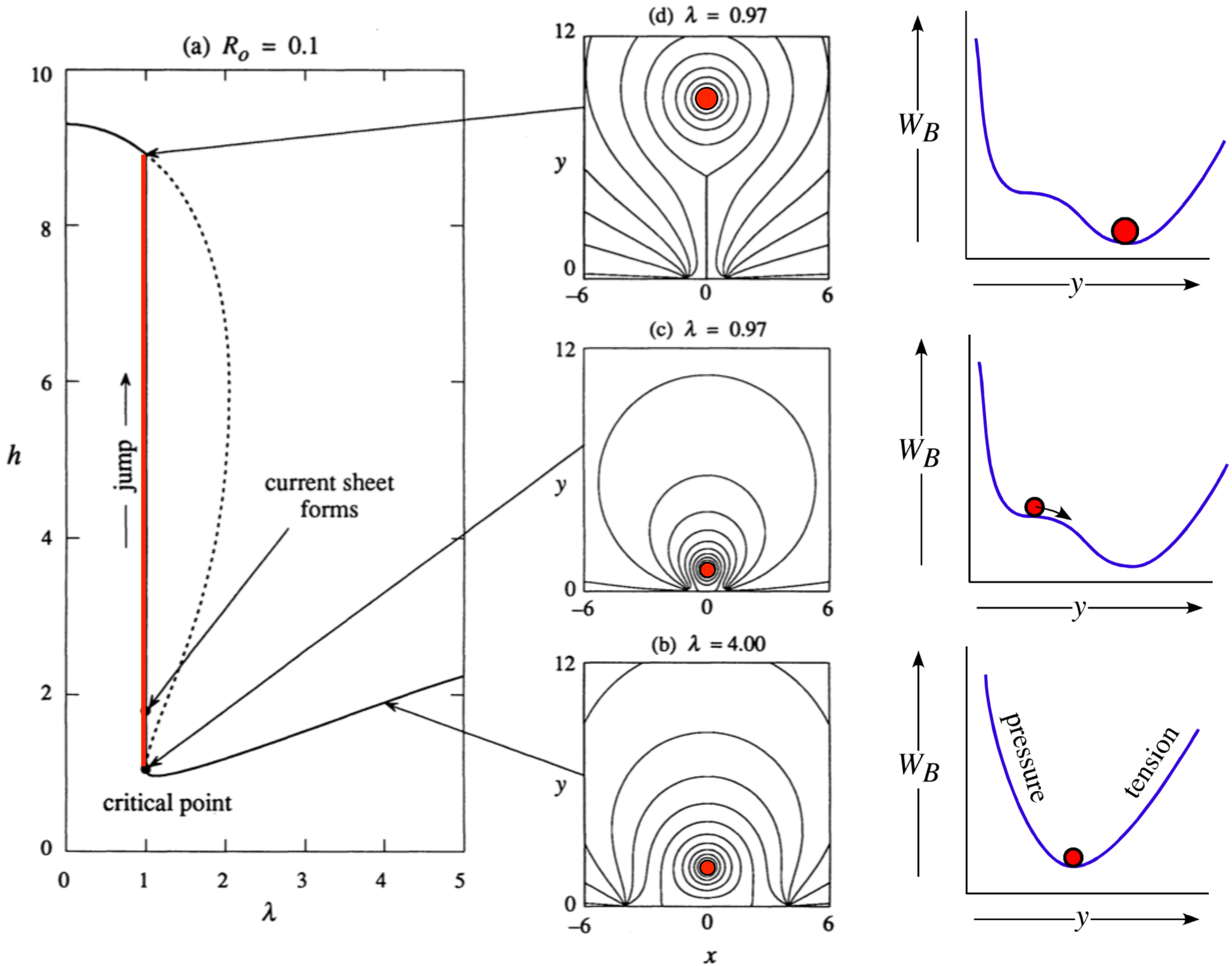

Energy Release in 2D Model

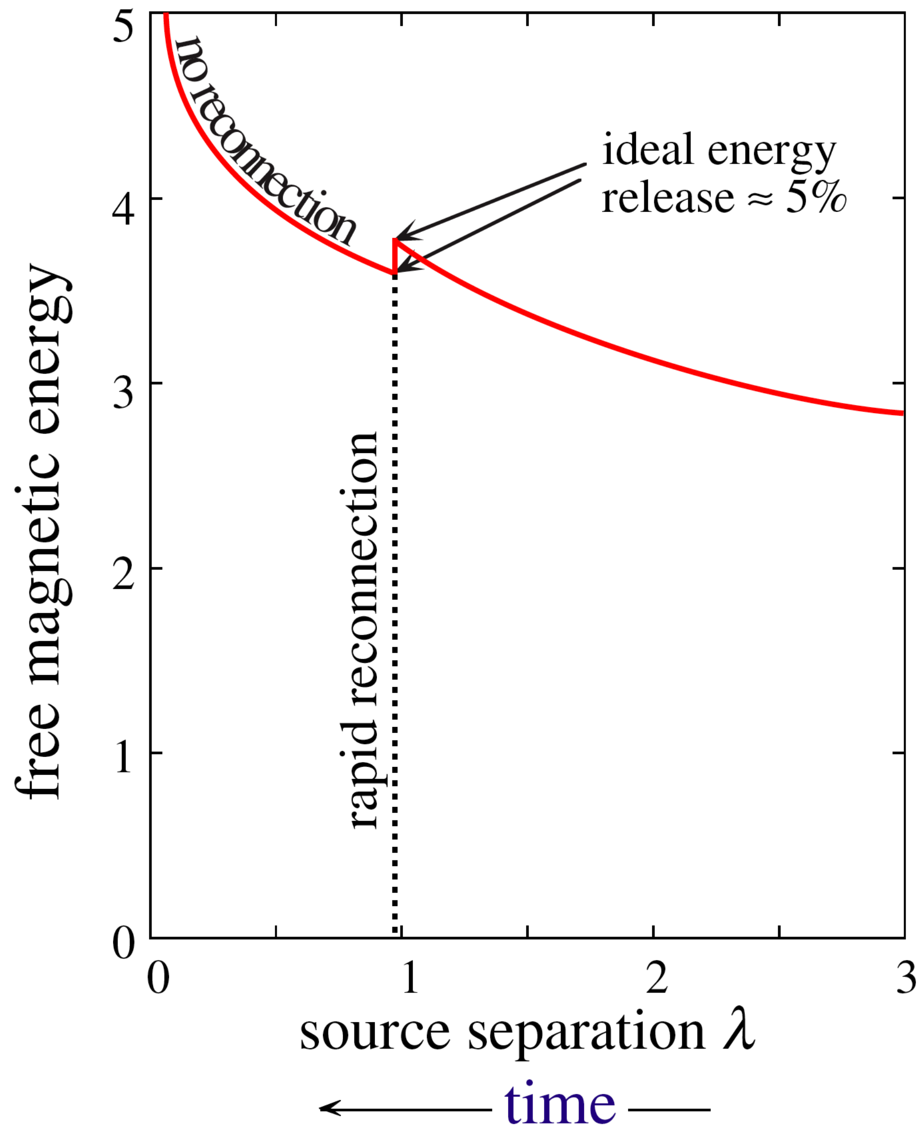

Trajectories

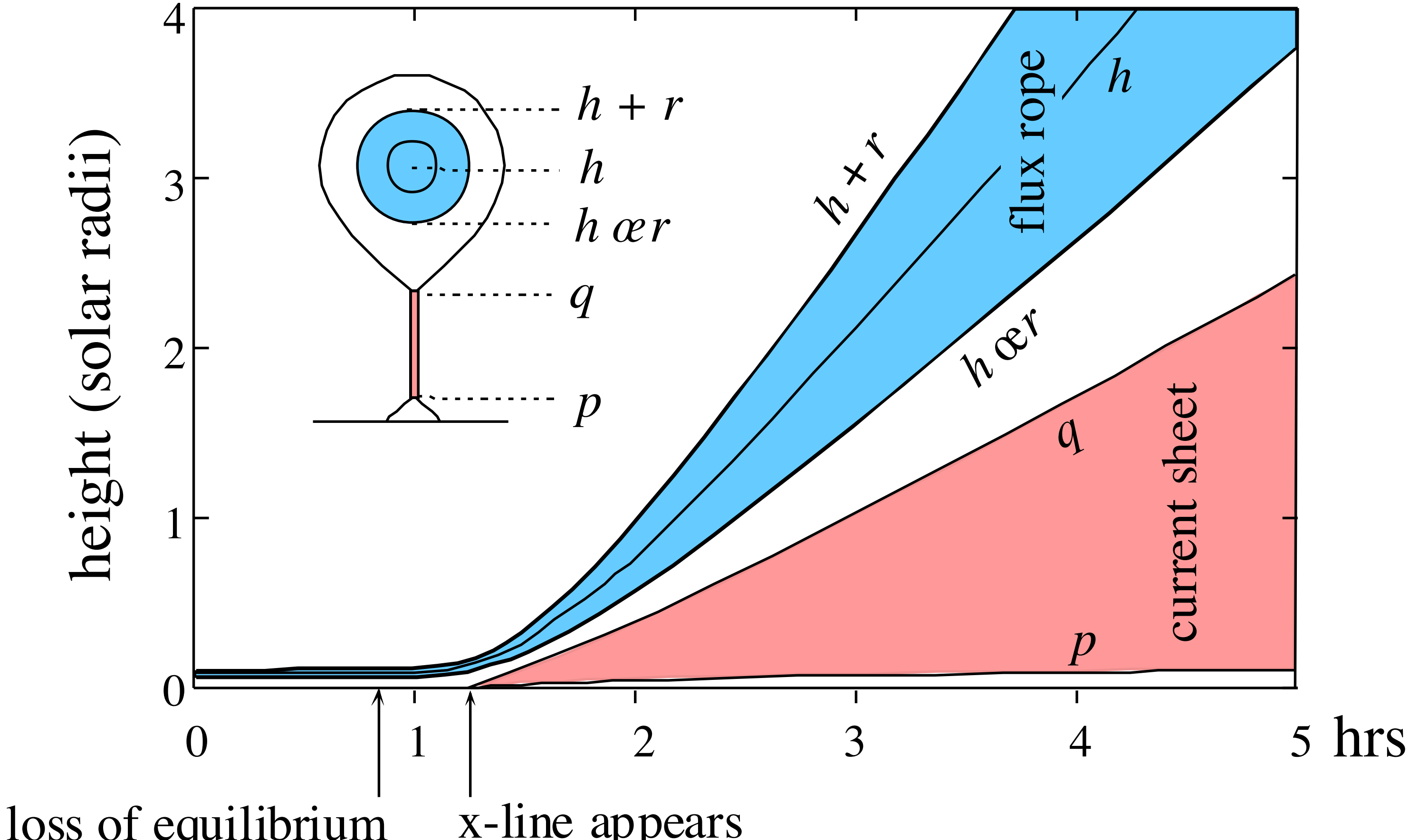

QuickTime™ and a
Animation decompressor
are needed to see this picture.

CME Energy Release versus Flare Energy Release

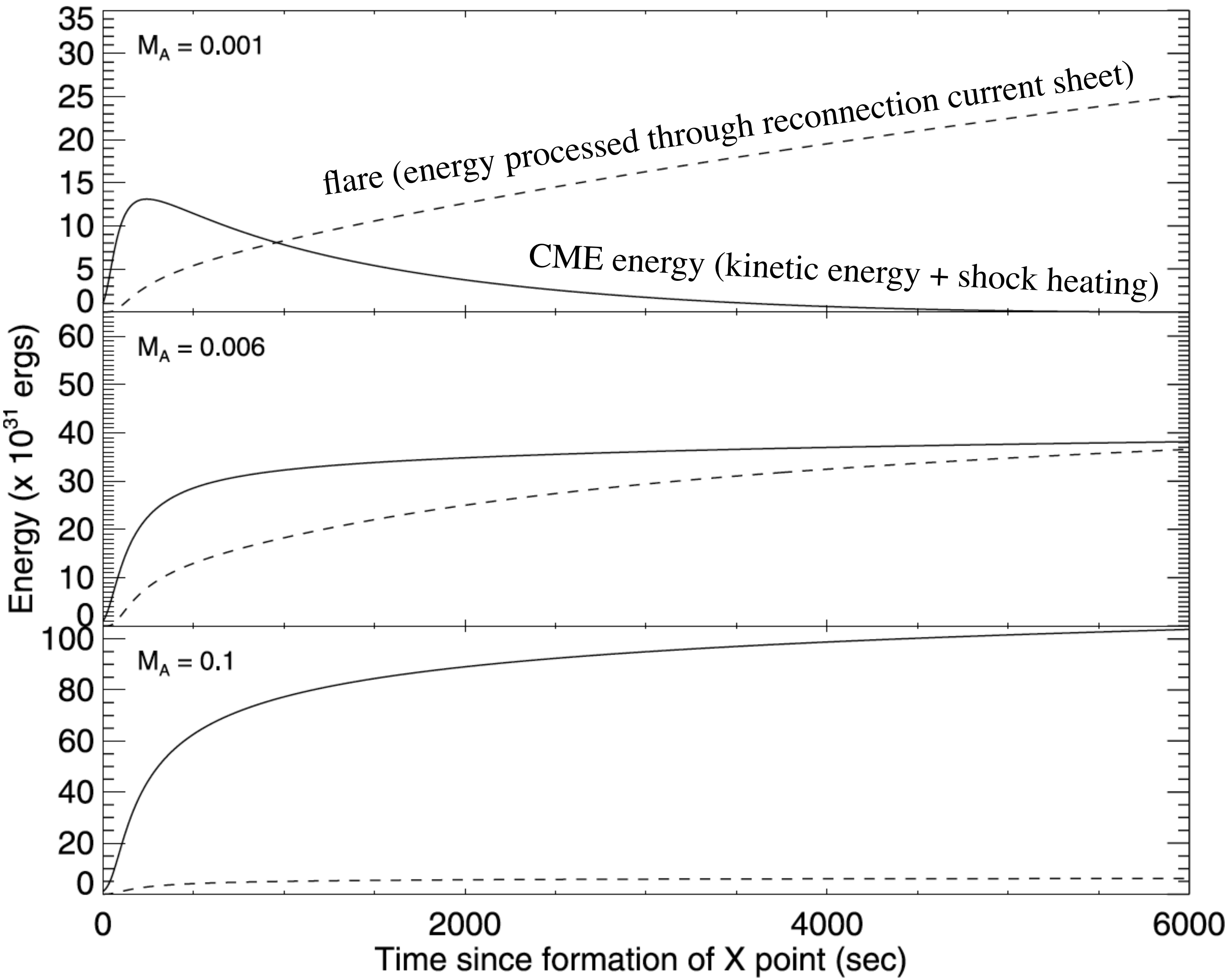

Power Production

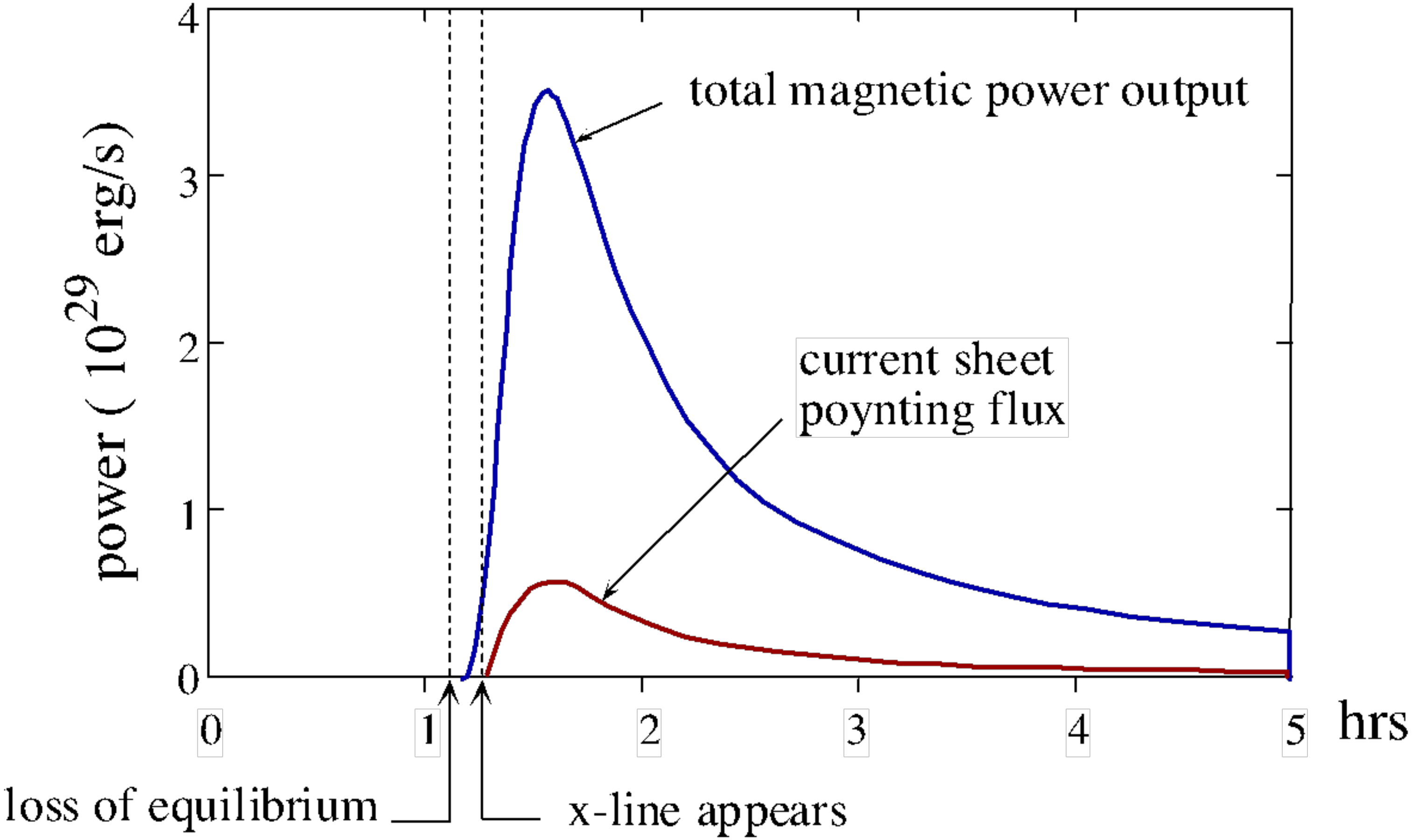

Numerical Simulation of Critical Point Configuration

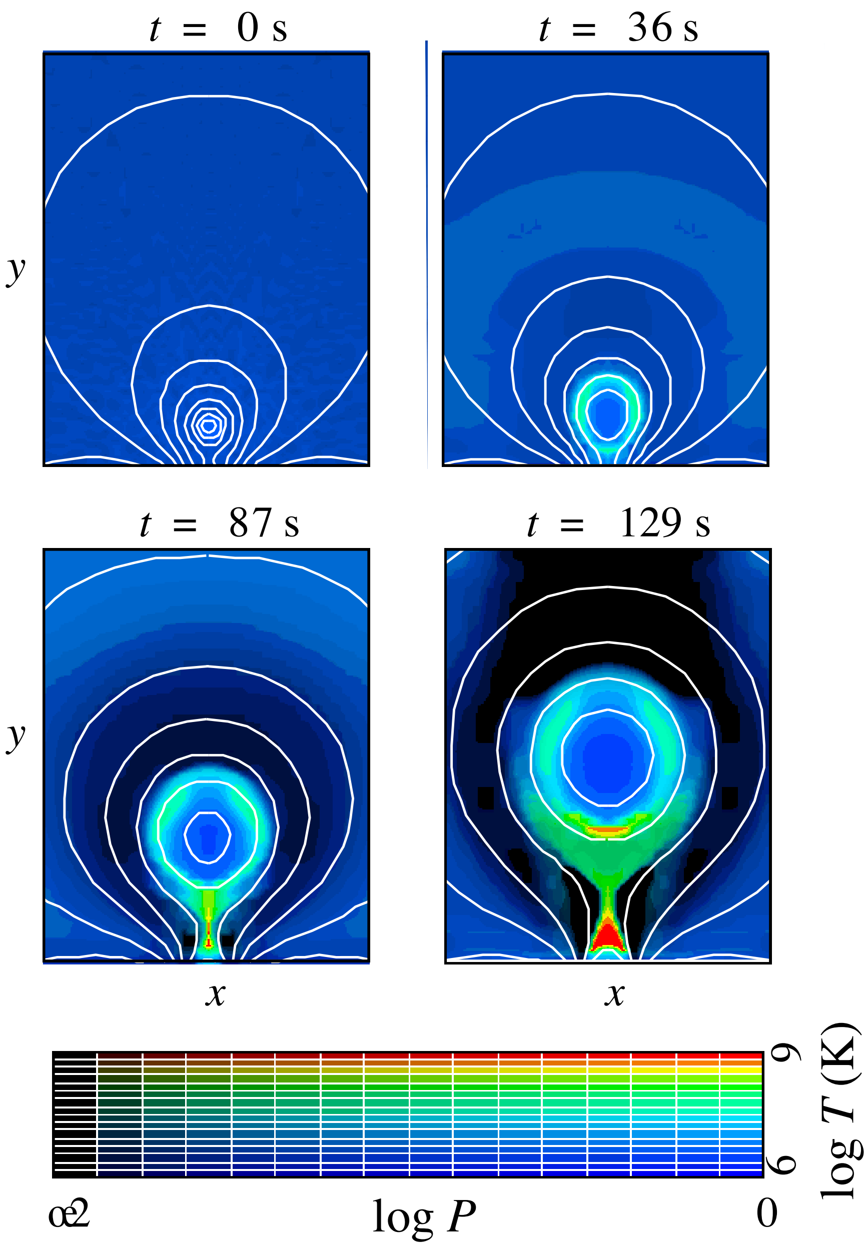

initial condition: $\mathbf{V} = 0$

energy equation: Ohmic heating
no cooling

resistivity: uniform, $S = 500$

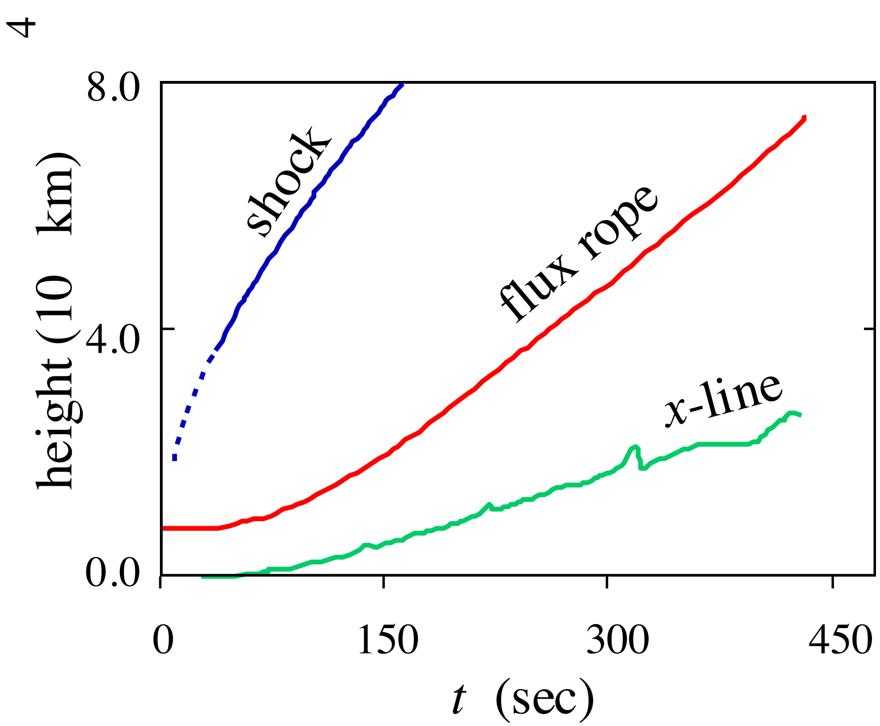

Basic Principles I

Driving Force:

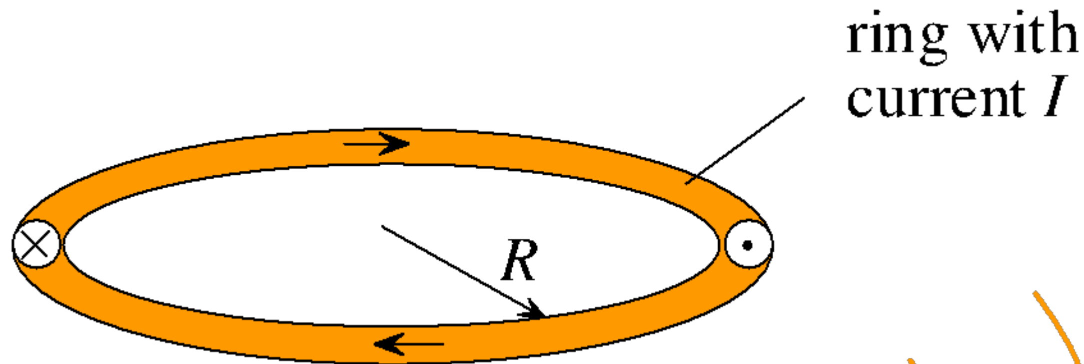

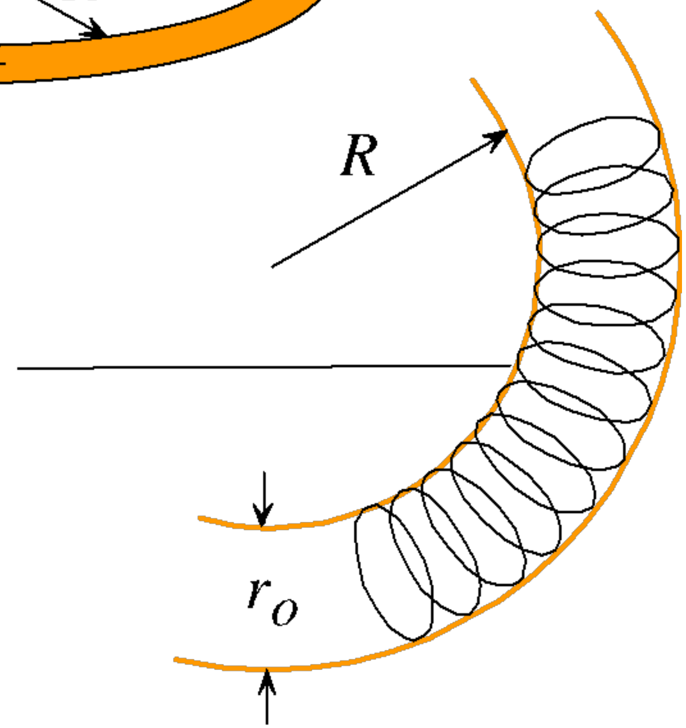

repulsive force:

$$\boxed{F \propto \frac{I^2}{R} \ln\left(R / r_o\right)}$$

Basic Principles II

Flux Conservation:

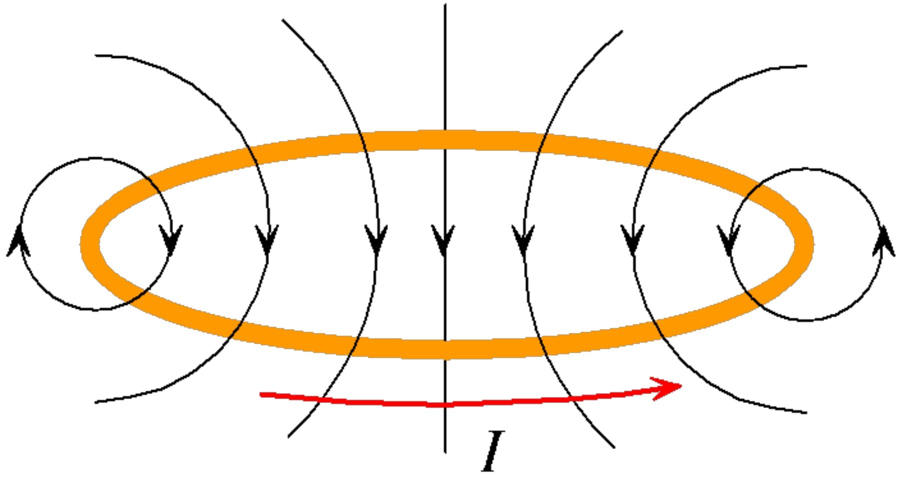

$$\boxed{I \propto 1/[R \ln(R/r_0)]}$$

How to Achieve Equilibrium

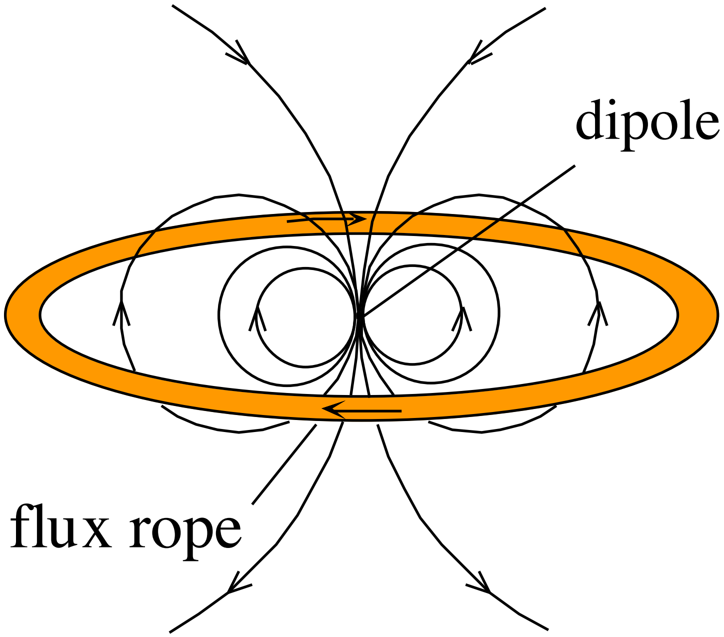

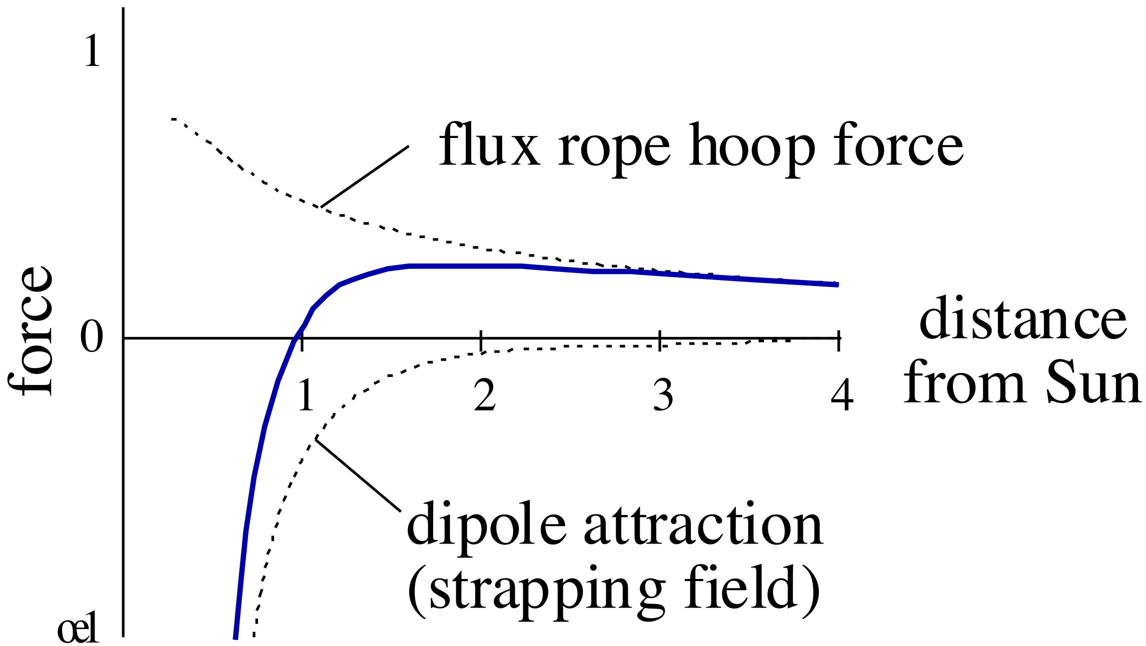

However, such an equilibrium is unstable!

How to Achieve a Stable Equilibrium

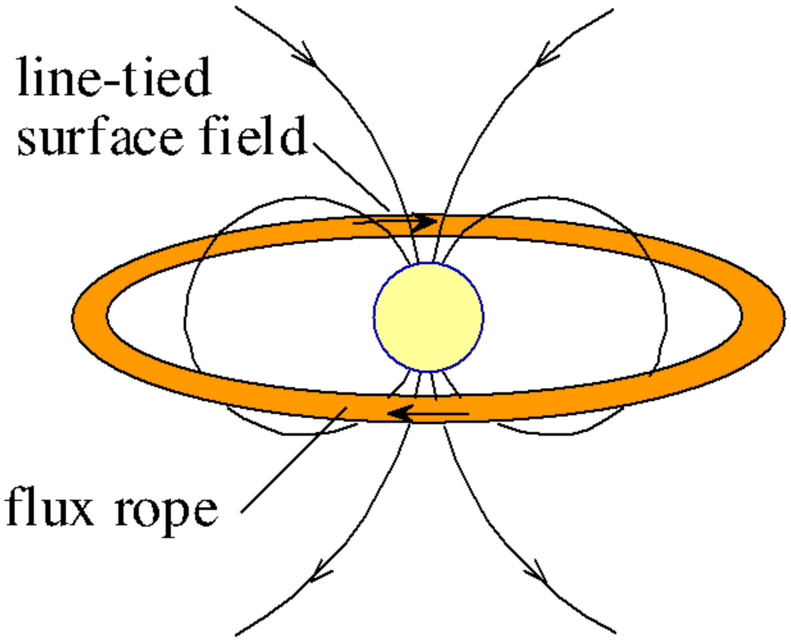

Key factor: Line-tying

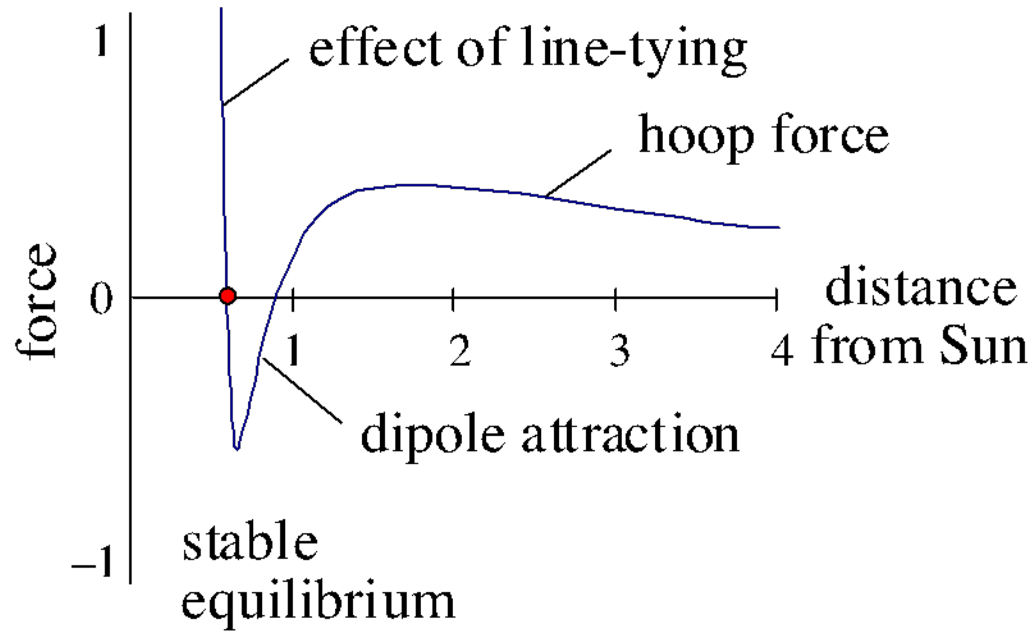

Line-tying creates a second, stable equilibrium

SAIC CME Simulation

QuickTime™ and a
Graphics decompressor
are needed to see this picture.

Linker et al. (2001)

3D Loss-of-Equilibrium Model

Titov & Démoulin (1999)

3 field sources

1. flux rope

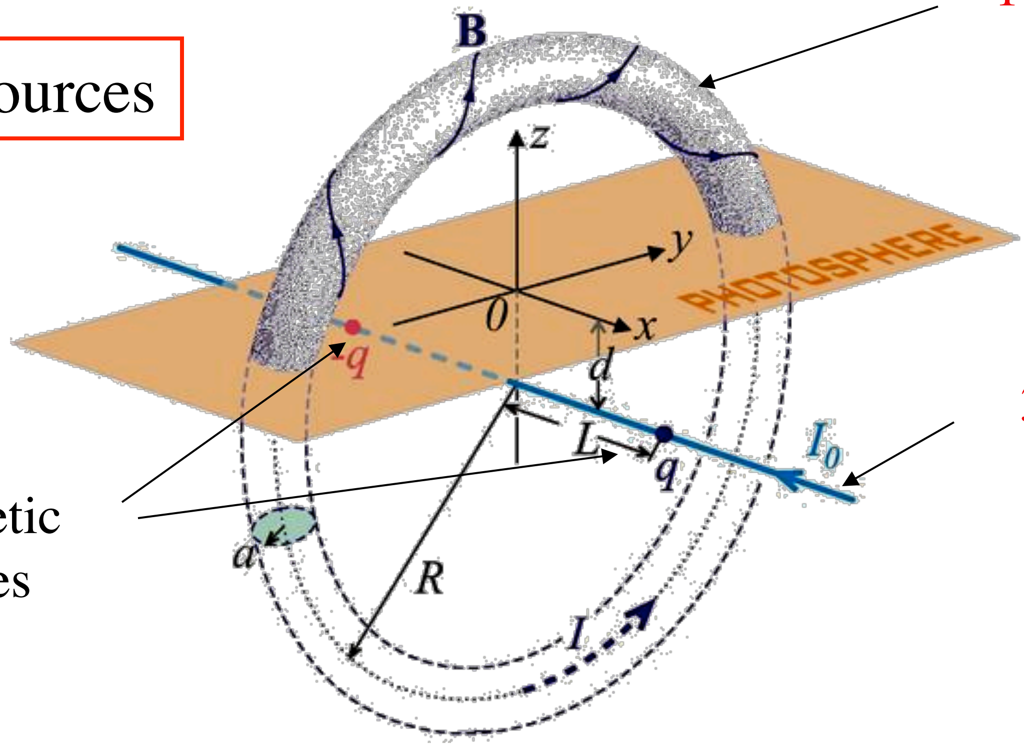

3. line-current

2. magnetic charges

IMF Trigger of Substorm

Substorm starts with and without IMF trigger

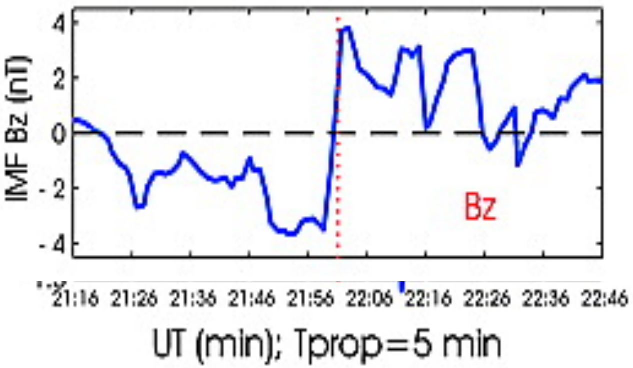

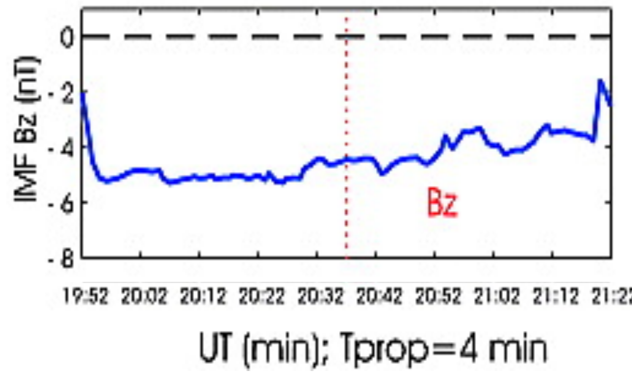

Substorm onset:
Internal instability.

But sensitive to change in convection

Triggered onset: 60% Non-triggered onset 40%

- IMF triggered substorms are stronger

→difficult to explain why magnetotail cannot store more energy when there is no trigger

tail Bz

Bt

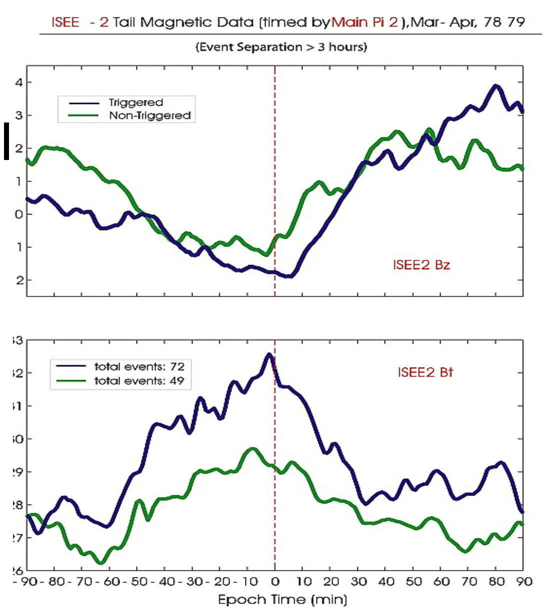

AL

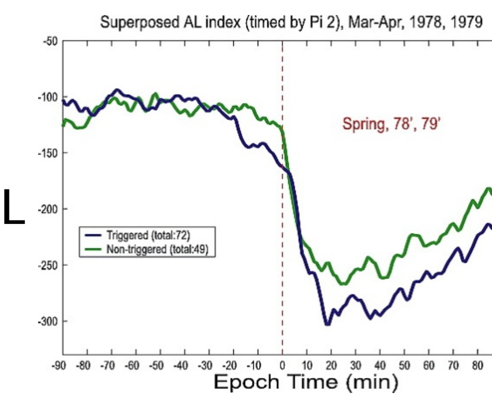

(Hsu and McPherron, 2004)

3D Line-Tied Solution by Method of Images

Solution for **B** in terms of incomplete elliptical integrals

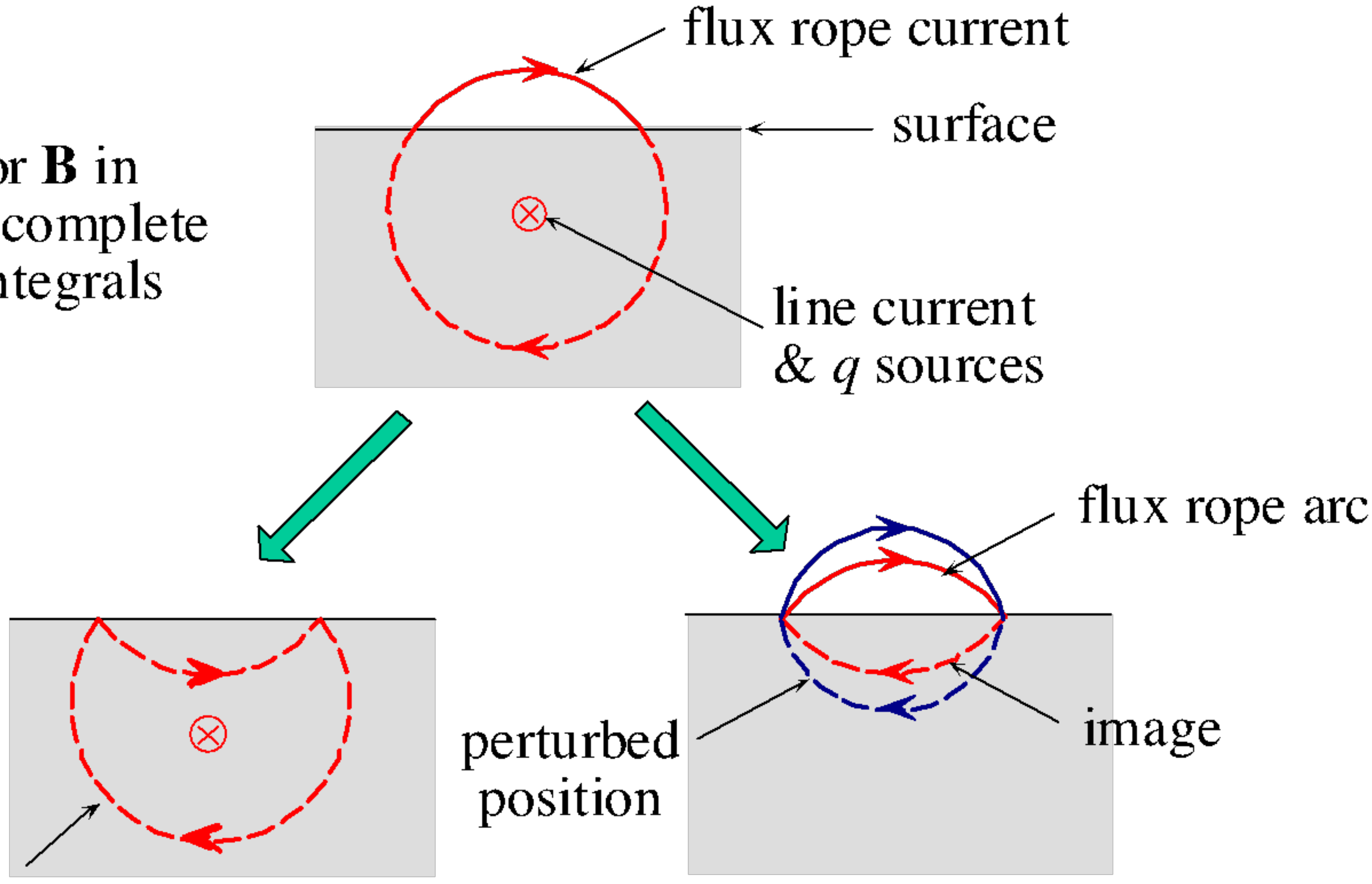

Line-Tied Evolution

erupted configuration

initial configuration

vertical field at surface

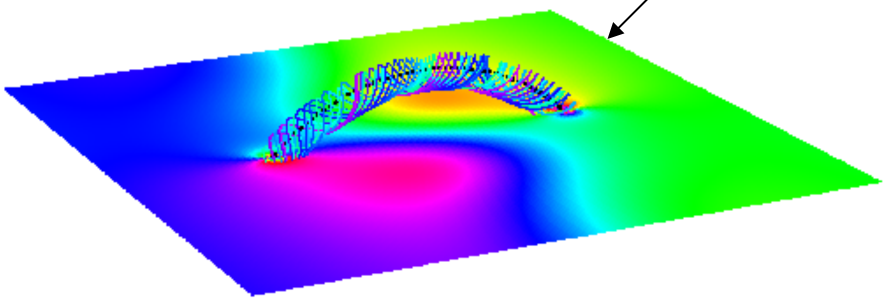

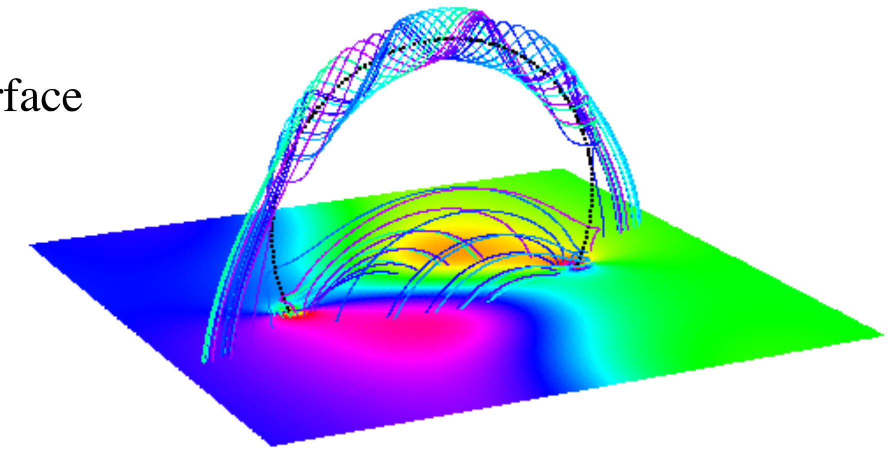

potential field

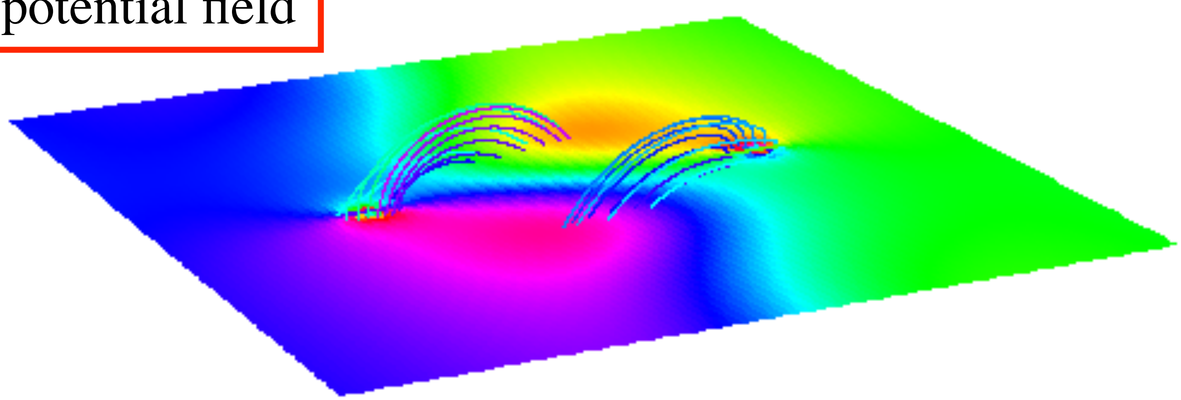

Flux-Rope Footprint

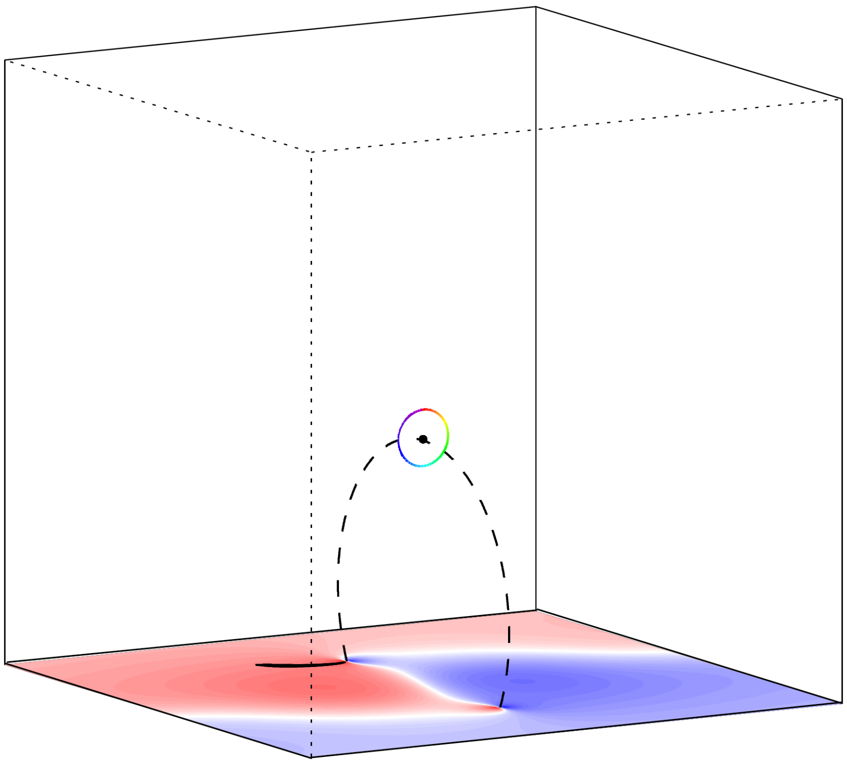

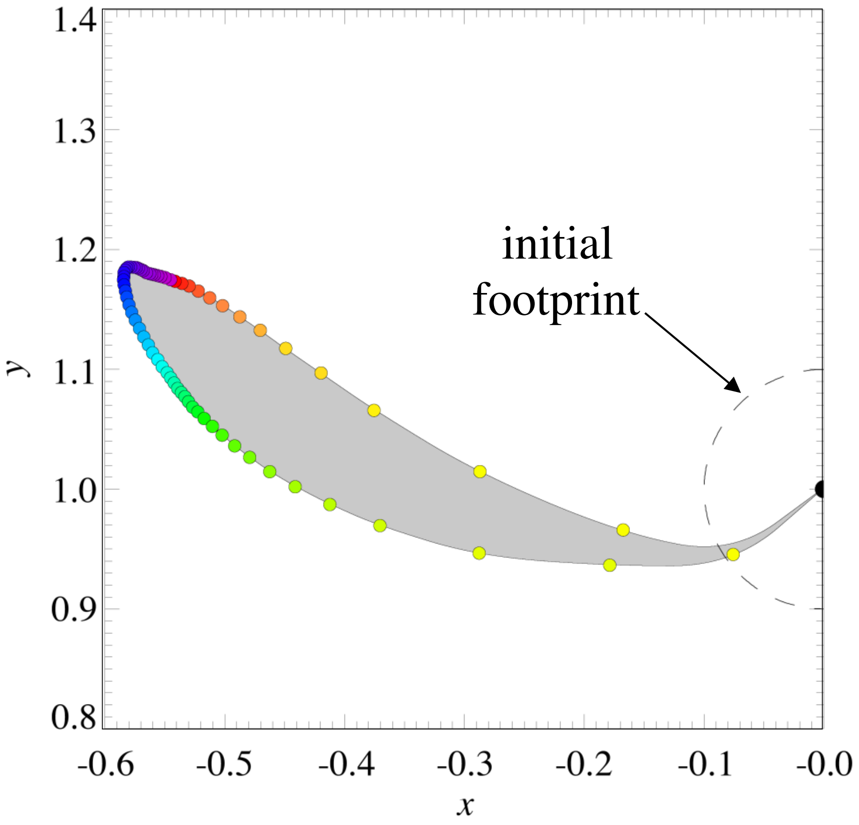

images courtesy of B. Kliem

Transient Coronal Holes as Seen by TRACE

QuickTime™ and a
Photo decompressor
are needed to see this picture.

Transient Coronal Holes as Seen by EIT

holes

QuickTime™ and a
TIFF (Uncompressed) decompressor
are needed to see this picture.

Transient Coronal Holes as Seen by EIT

QuickTime™ and a
GIF decompressor
are needed to see this picture.

Transient Coronal Holes as Seen by EIT

QuickTime™ and a
PNG decompressor
are needed to see this picture.

Forces Acting on Flux Rope

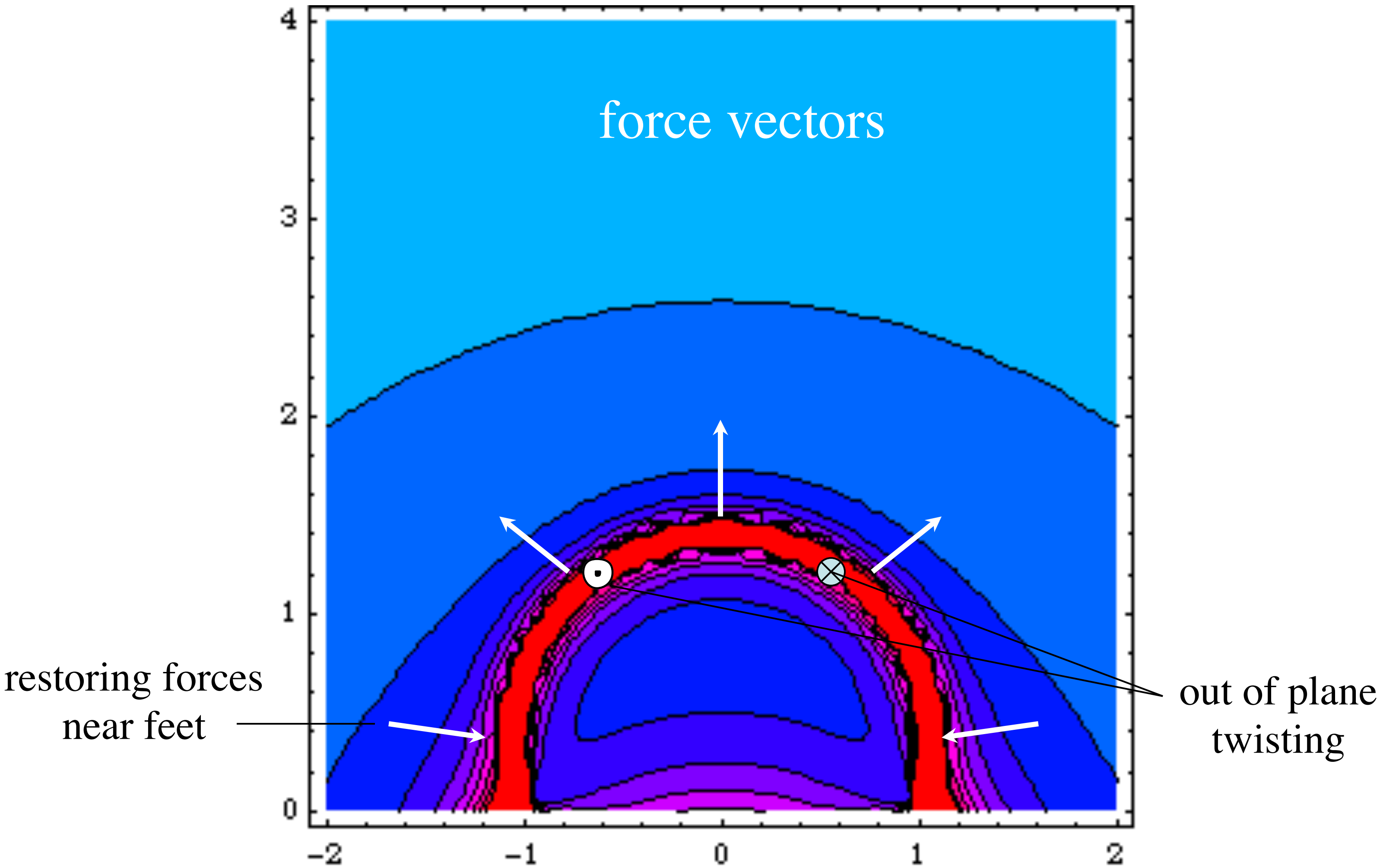

current density

QuickTime™ and a
GIF decompressor
are needed to see this picture.

QuickTime™ and a
Photo decompressor
are needed to see this picture.

Kliem & Török (2004)

Simulation of Kliem & Török

QuickTime™ and a
GIF decompressor
are needed to see this picture.

1. line current replaced by quadrupole
2. subcritical twist for helical kink
3. torus center near surface

What is the Trigger Mechanism in the Breakout Model?

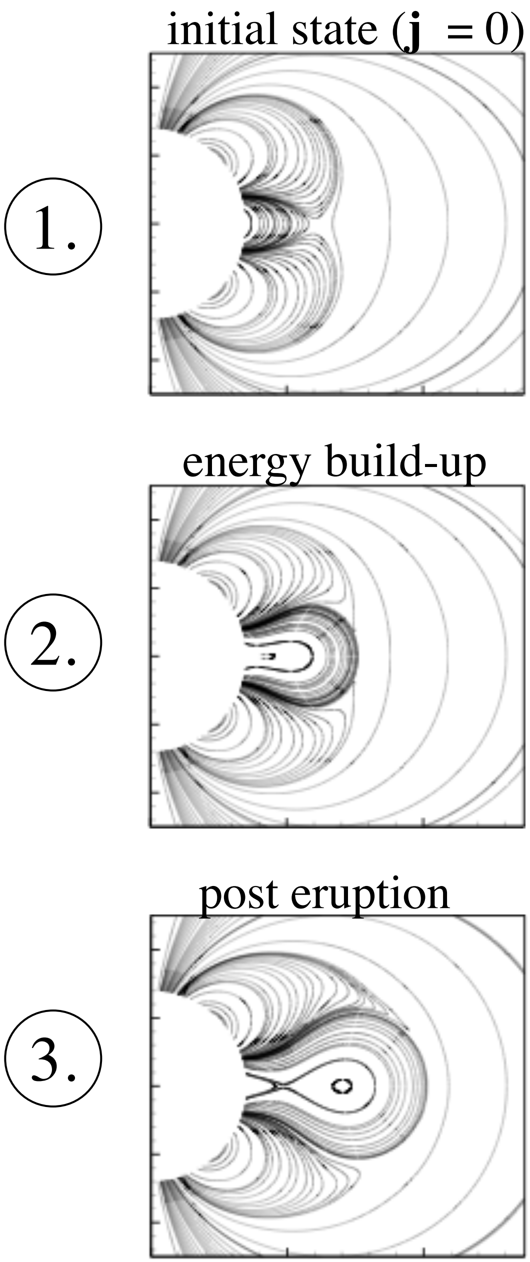

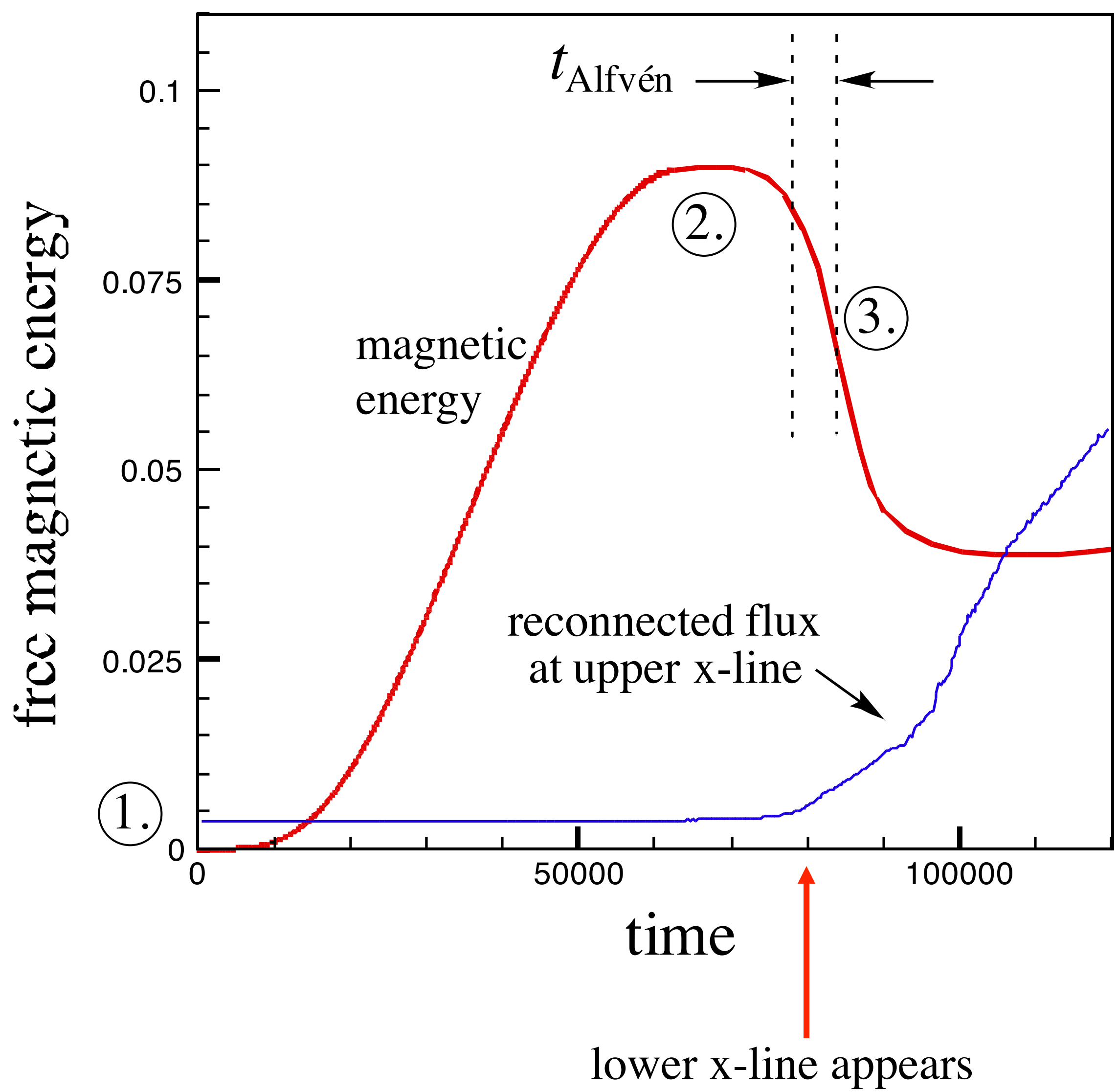

Role of Reconnection in the Breakout Model

QuickTime™ and a
decompressor
are needed to see this picture.

QuickTime™ and a
BMP decompressor
are needed to see this picture.

Flux Rope Emergence & Eruption

QuickTime™ and a
BMP decompressor
are needed to see this picture.

QuickTime™ and a
GIF decompressor
are needed to see this picture.

3D simulations of Fan & Gibson (2006)

Flux Ropes Are Characteristic of Low β Plasmas

van Ballegooijen & Mackay 2007

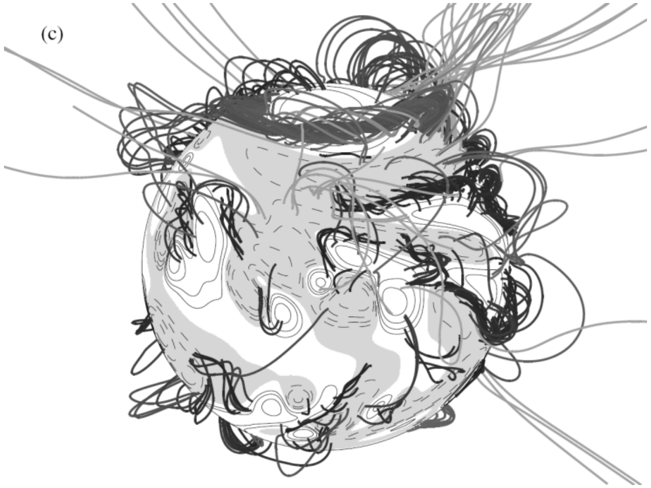

prominence plasma $\beta << 1$

$$\nabla P \approx 0 \; : \; \mathbf{j} \times \mathbf{B} \approx 0 \qquad \mathbf{j} \parallel \mathbf{B}$$

j along **B** produces twist

flux rope defined as enough twist to produce inverse polarity

(about 1 turn)

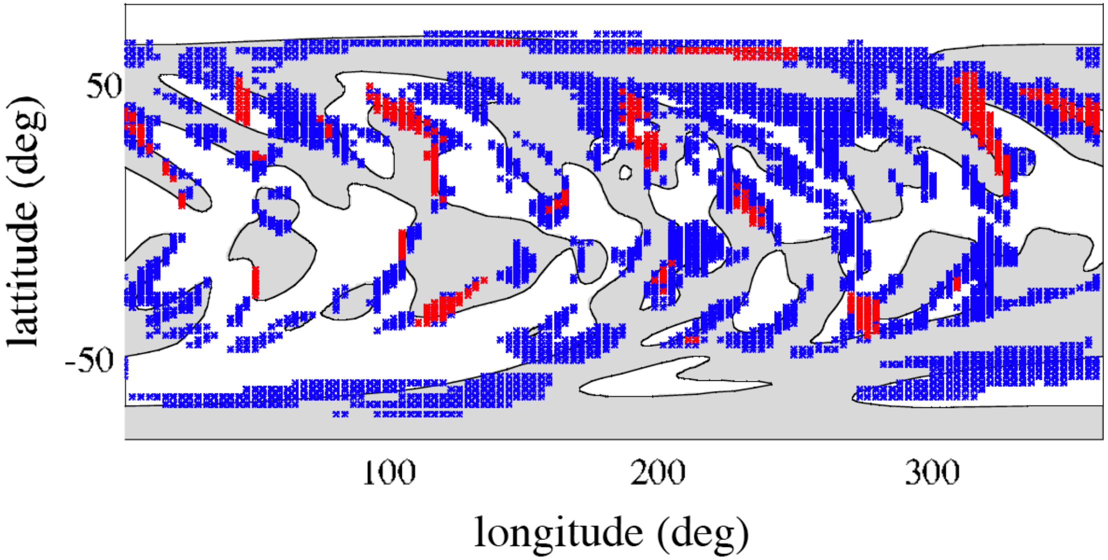

blue: flux ropes

red: flux ropes that erupted

Yeates & Mackay 2009

Recovery

Reconnection Electric Fields

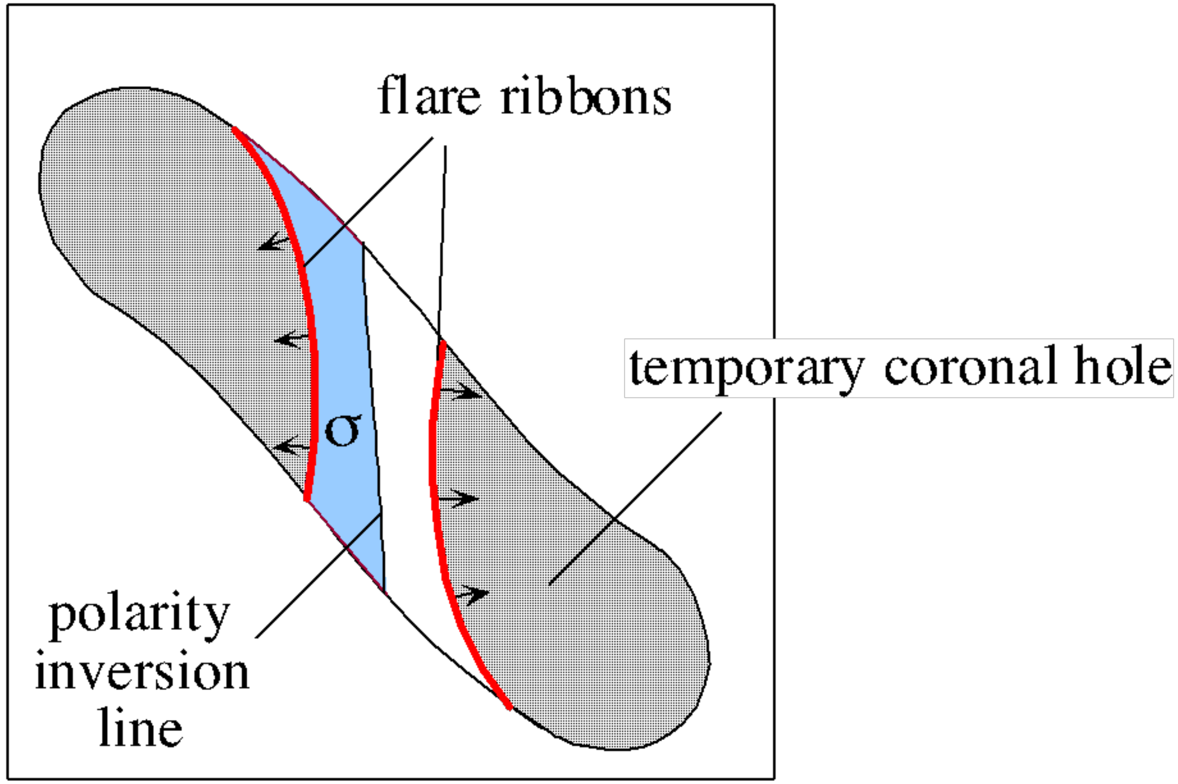

newly reclosed flux:

$$\Phi_B = \iint_{\sigma} B_z \, dxdy$$

global reconnection rate:

$$\int \mathbf{E} \cdot \mathbf{dl} = \frac{d\Phi_b}{dt}$$

QuickTime™ and a
TIFF (Uncompressed) decompressor
are needed to see this picture.

CME/Flare Reconnection Rate

Observed Reconnection Rate for X3 Flare

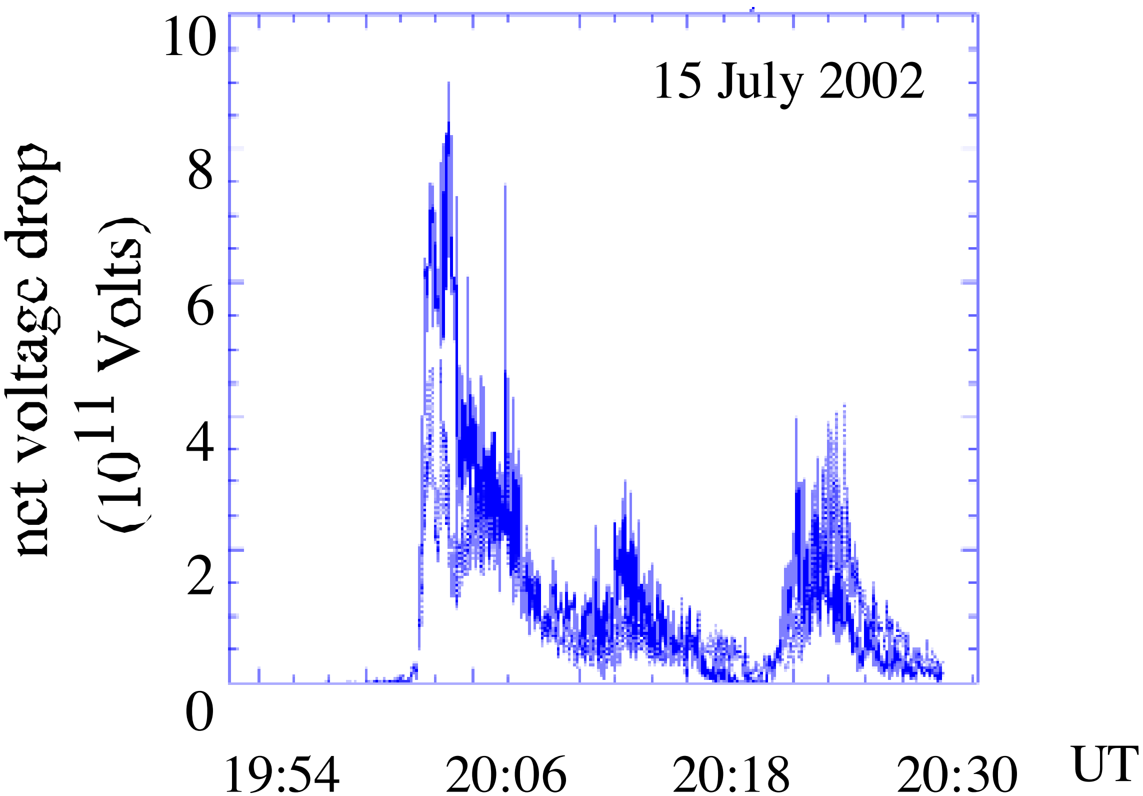

$$E_{\text{reconnect}} \,/\, E_{\text{Dreicer}} \;=\; 10^{6} \;\; \gg 1$$

collisionless processes involved

Substorm Reconnection Rate

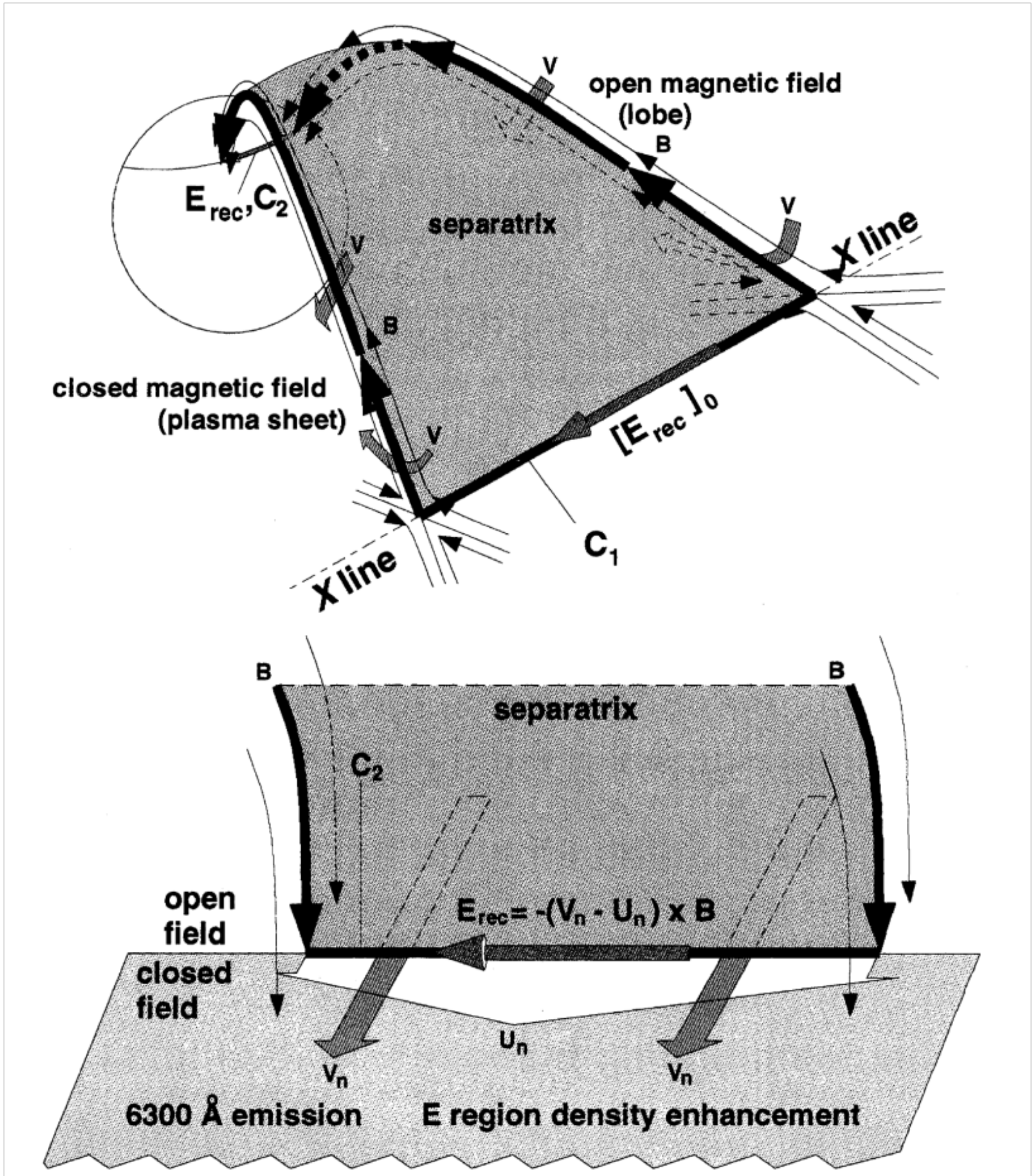

$$\int_{C_1} \left[\mathbf{E}_{\mathbf{rec}}\right]_0 \cdot \mathbf{dl} = \int_{C_2} B(V_n - U_n)dl$$

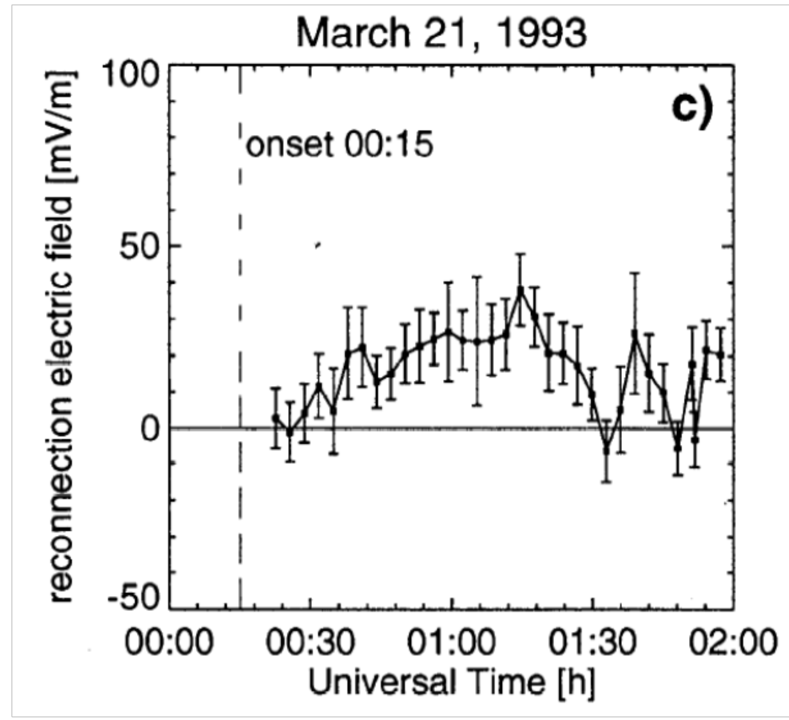

Blanchard et al. (1996)

2D Numerical Simulation of Flare Reconnection

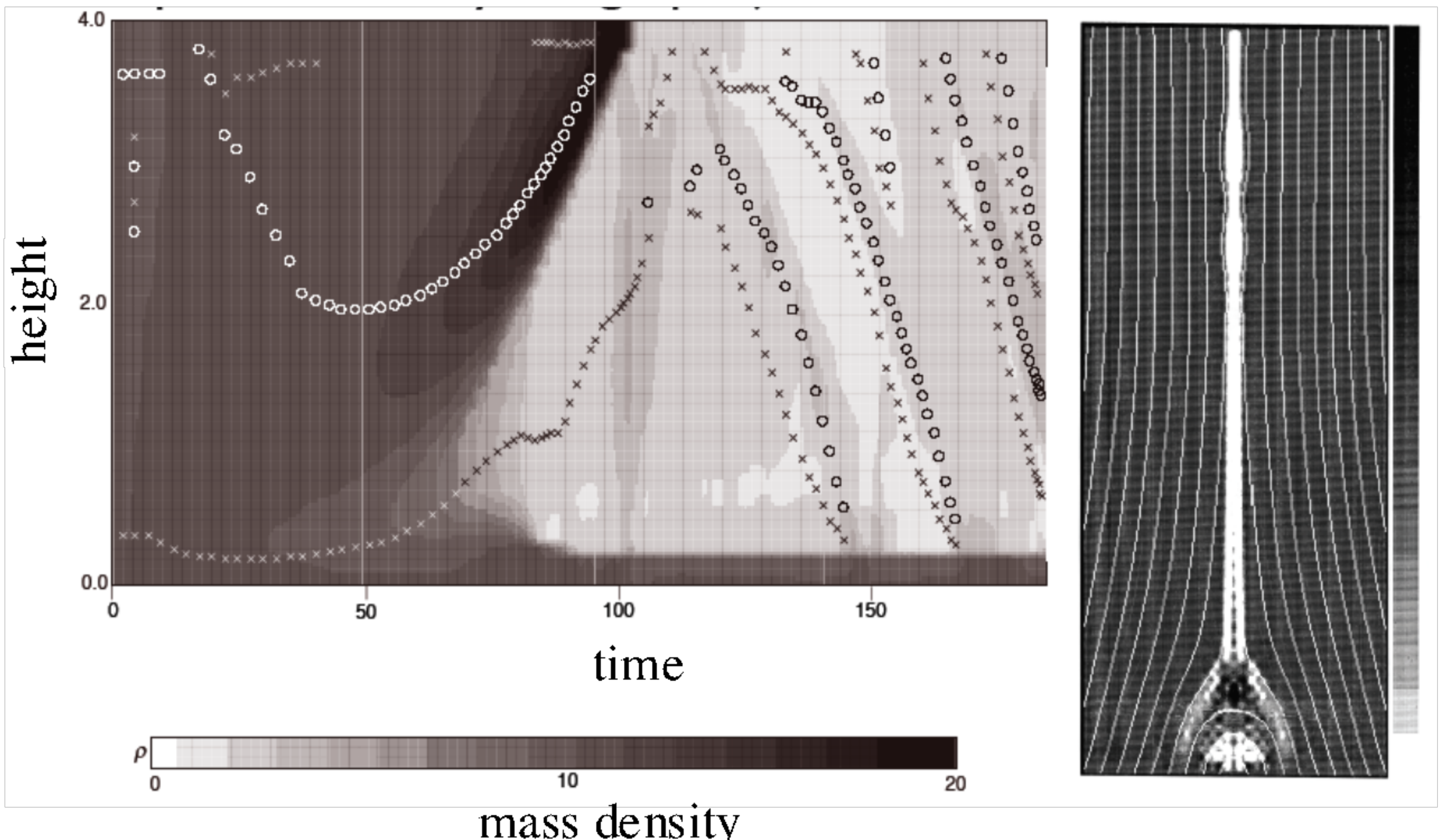

MHD Simulation of Line-Tied Current Sheet

QuickTime™ and a
decompressor
are needed to see this picture.

Shen et al. 2008

Aurora and Bursty Bulk Flows

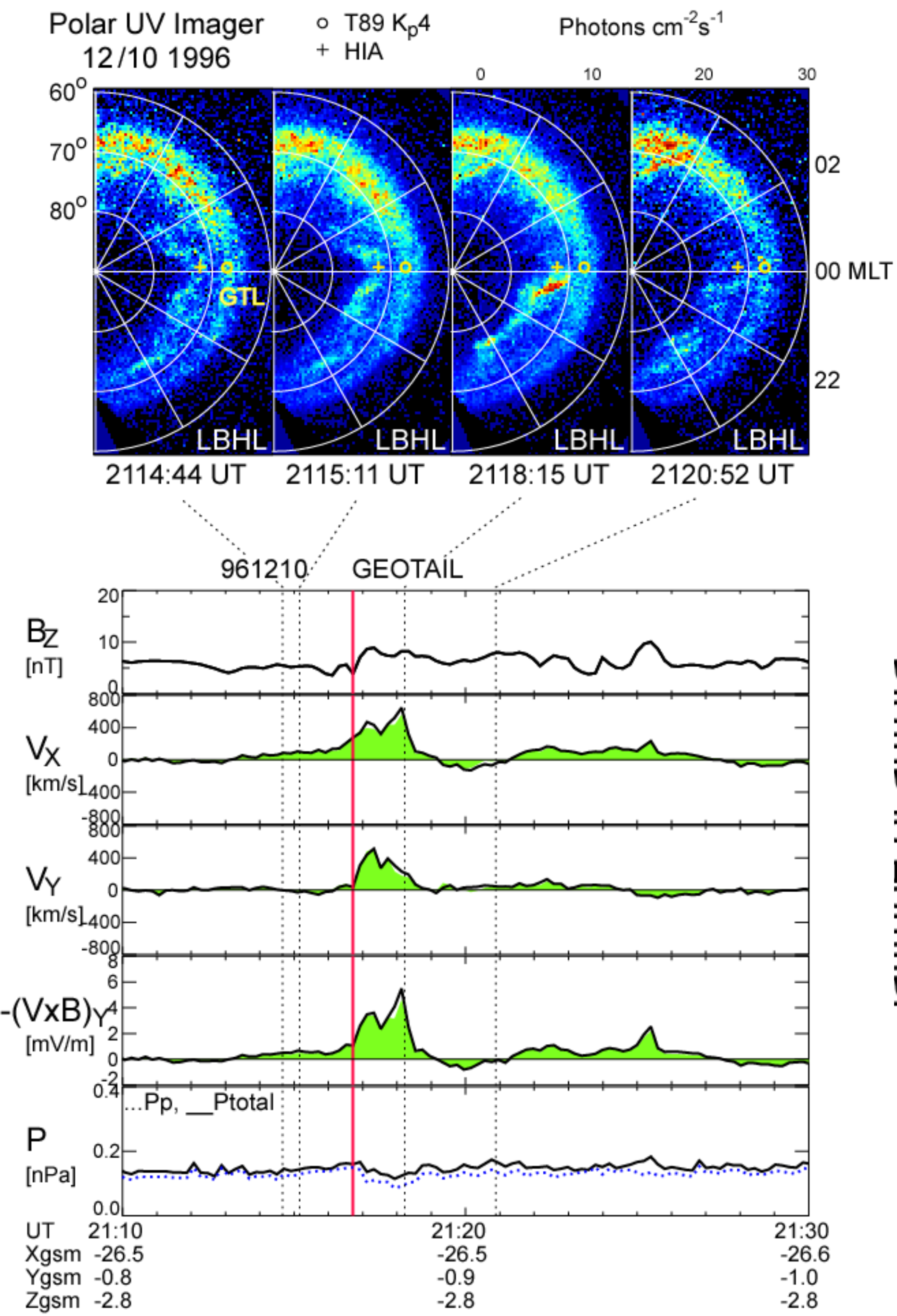

Isolated flow bursts with > 2 mV/m (Geotail) correspond to auroral activations

Auroral activations near foot point of satellite start within 1 min of flow burst onset.

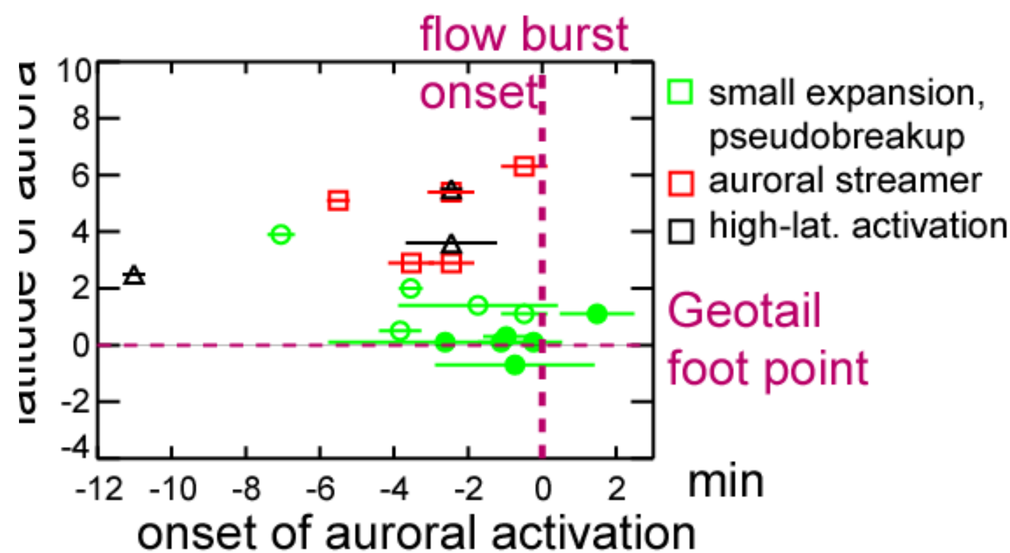

Nakamura et al., 2001

Evidence of Bursty Reconnection in CMEs/Flares

QuickTime™ and a
Photo decompressor
are needed to see this picture.

- High speed (400 km/s) downflows observed above flare loops.
- Multiple island-like structures (“tadpoles” / SADs).

2D MHD Simulation of Late Phase Reconnection

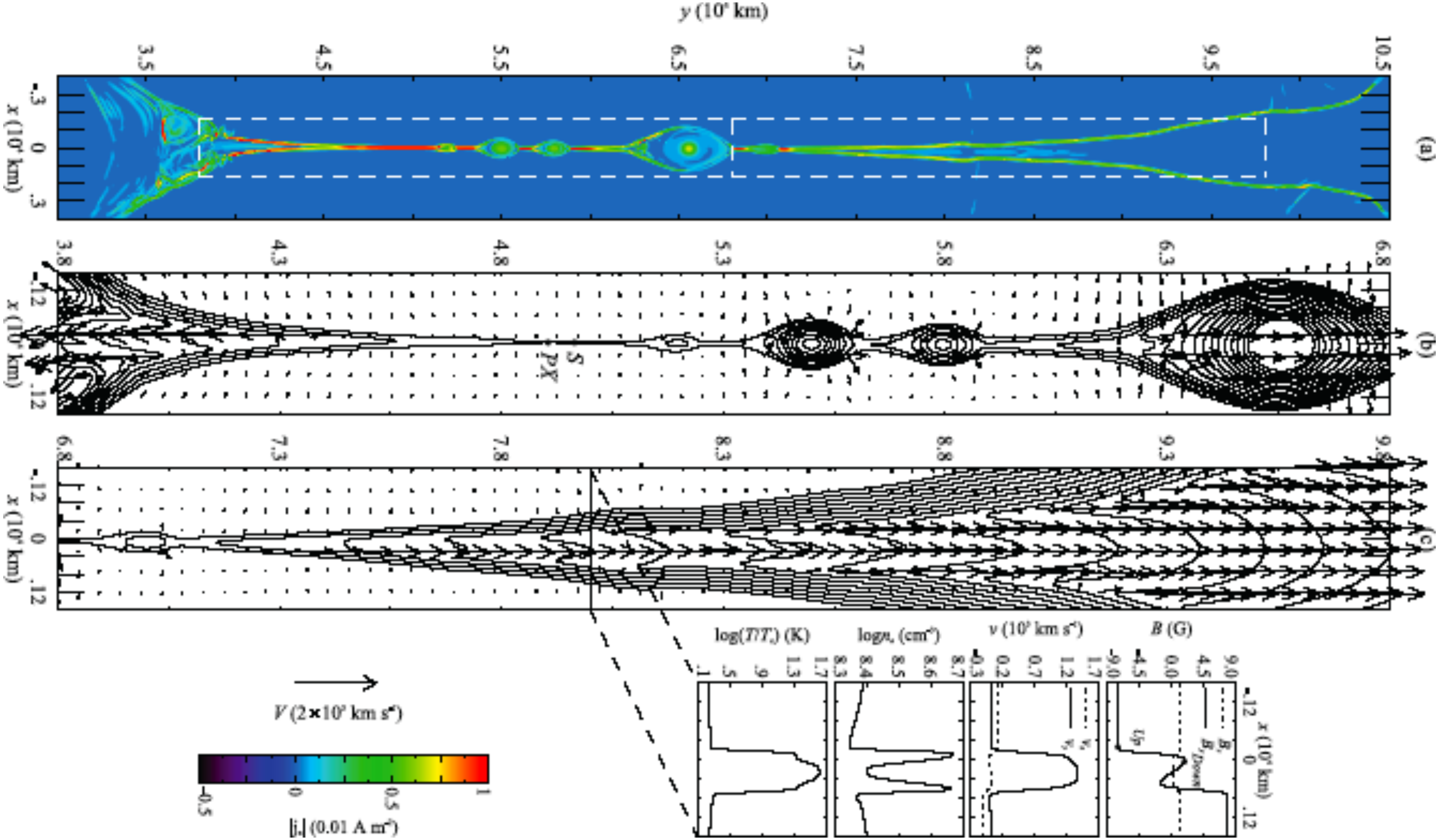

Mei et al. 2012

Tracking of Small Features in Current Sheet

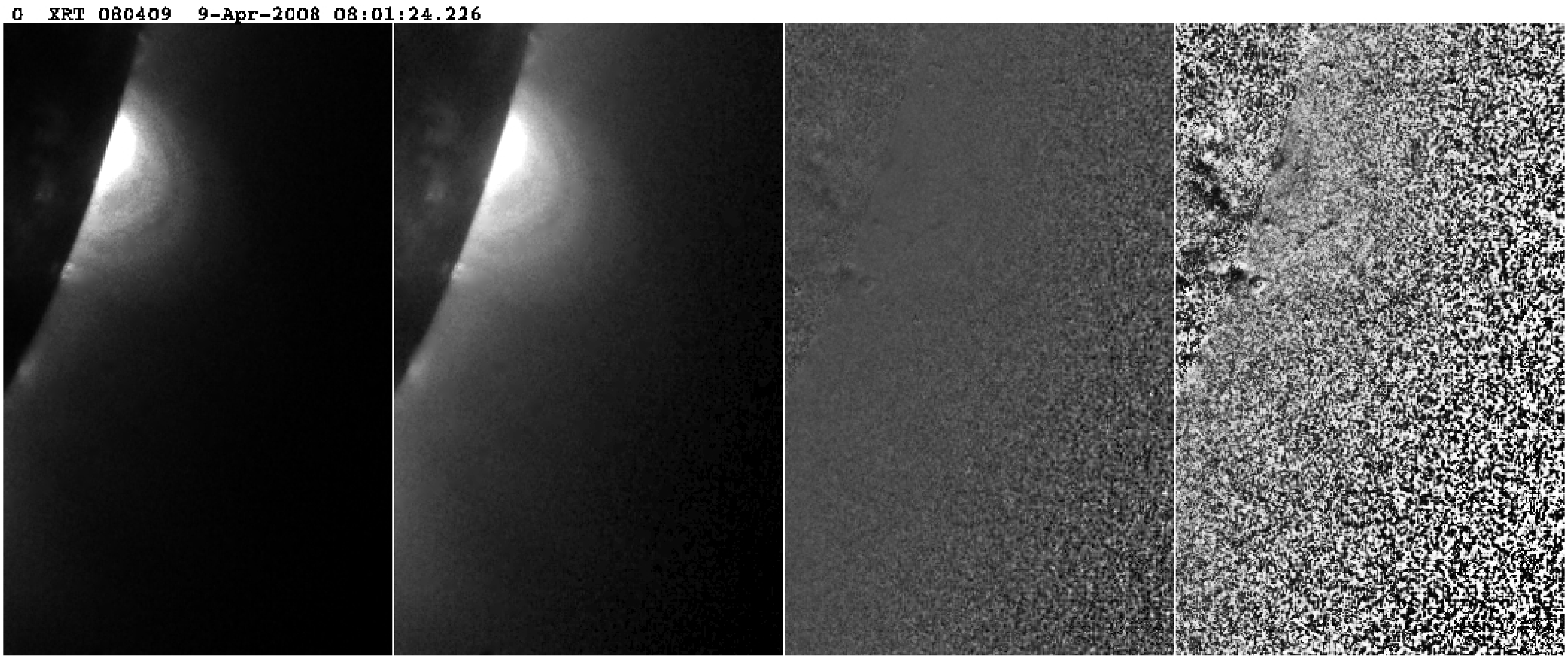

Propagation of XRT Features into LASCO Field of View

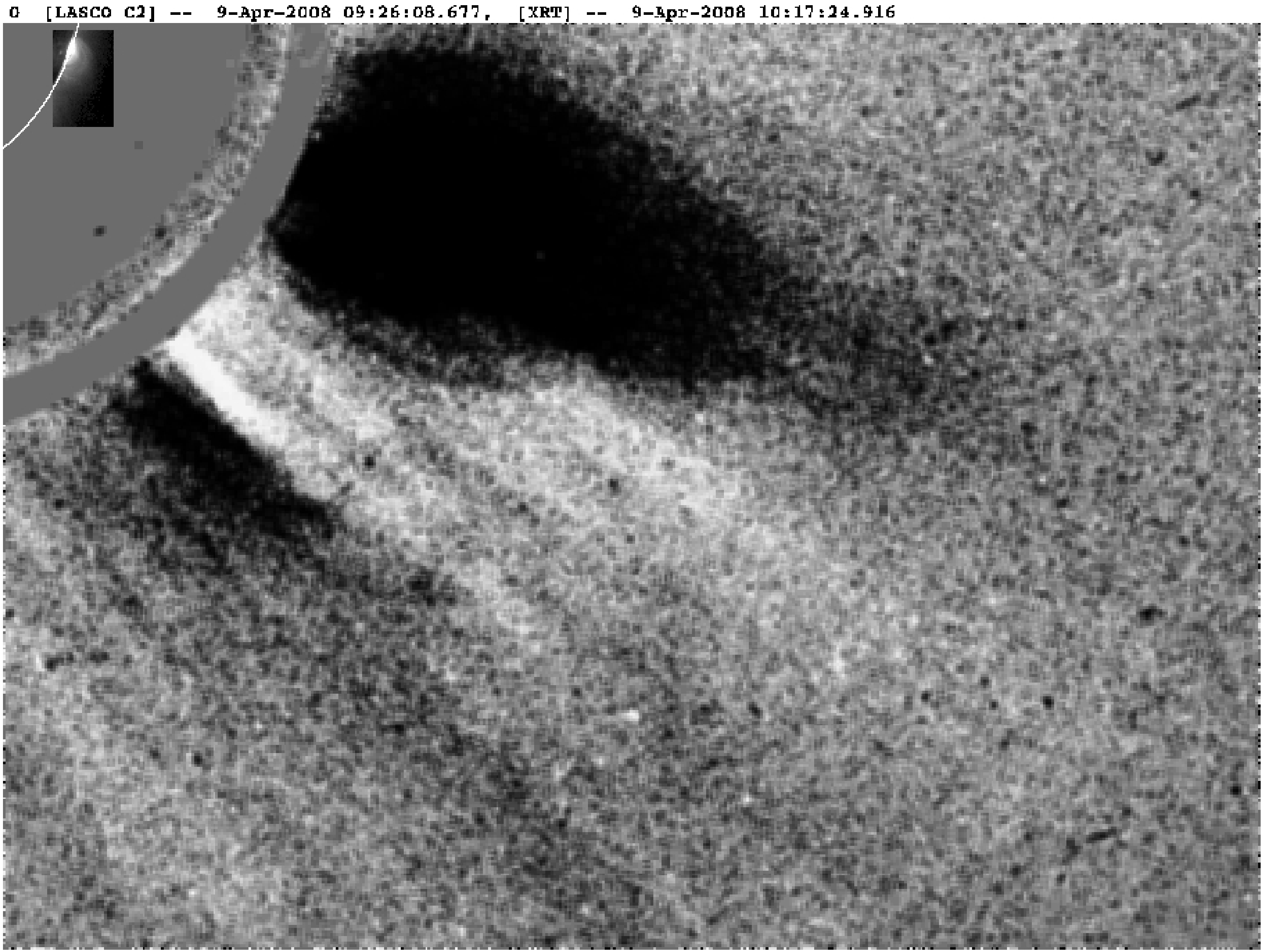

Energy Phases

1. Growth Phase

   magnetospheric: creation of tail current sheet, well understood

   solar: force-free currents, subsurface, poorly understood

2. Onset Mechanism

   magnetospheric: kinetic versus ideal-MHD process

   solar: kinetic versus ideal-MHD process, hybrid process

3. Energy Release

   magnetospheric: current sheet dynamics, ionosphere

   solar: current sheet dynamics, thermal conduction, radiation